

An interatomic potential for saturated hydrocarbons based on the modified embedded-atom method

S. Nouranian,¹ M.A. Tschopp,^{1,2} S.R. Gwaltney,³ M.I. Baskes,⁴ and M.F. Horstemeyer^{1,5}

¹*Center for Advanced Vehicular Systems (CAVS),*

Mississippi State University, Mississippi State, MS 39762, USA

²*Dynamic Research Corporation, (on site at) U.S. Army Research Laboratory,
Aberdeen Proving Ground, MD 21005, USA*

³*Department of Chemistry, Mississippi State University, Mississippi State, MS 39762, USA*

⁴*Department of Aerospace Engineering,
Mississippi State University, Mississippi State, MS 39762, USA*

⁵*Department of Mechanical Engineering,
Mississippi State University, Mississippi State, MS 39762, USA*

Abstract

In this work, we developed an interatomic potential for saturated hydrocarbons using the modified embedded-atom method (MEAM), a reactive semi-empirical many-body potential based on density functional theory and pair potentials. We parameterized the potential by fitting to a large experimental and first-principles (FP) database consisting of 1) bond distances, bond angles, and atomization energies at 0 K of a homologous series of alkanes and their select isomers from methane to *n*-octane, 2) the potential energy curves of H₂, CH, and C₂ diatomics, 3) the potential energy curves of hydrogen, methane, ethane, and propane dimers, i.e., (H₂)₂, (CH₄)₂, (C₂H₆)₂, and (C₃H₈)₂, respectively, and 5) pressure-volume-temperature (*PVT*) data of a dense high-pressure methane system with the density of 0.5534 g/cc. We compared the atomization energies and geometries of a range of linear alkanes, cycloalkanes, and free radicals calculated from the MEAM potential to those calculated by other commonly used reactive potentials for hydrocarbons, i.e., second-generation reactive empirical bond order (REBO) and reactive force field (ReaxFF). MEAM reproduced the experimental and/or FP data with accuracy comparable to or better than REBO or ReaxFF. The experimental *PVT* data for a relatively large series of methane, ethane, propane, and butane systems with different densities were predicted reasonably well by MEAM. Although the MEAM formalism has been applied to atomic systems with predominantly metallic bonding in the past, the current work demonstrates the promising extension of the MEAM potential to covalently bonded molecular systems, specifically saturated hydrocarbons and saturated hydrocarbon-based polymers. The MEAM potential has already been parameterized for a large number of metallic unary, binary, ternary, carbide, nitride, and hydride systems, and extending it to saturated hydrocarbons provides a reliable and transferable potential for atomistic/molecular studies of complex material phenomena involving hydrocarbon-metal or polymer-metal interfaces, polymer-metal nanocomposites, fracture and failure in hydrocarbon-based polymers, etc. The latter is especially true since MEAM is a reactive potential that allows for dynamic bond formation and bond breaking during simulation. Our results show that MEAM predicts the energetics of two major chemical reactions for saturated hydrocarbons, i.e., breaking a C-C and a C-H bond, reasonably well. However, the current parameterization does not accurately reproduce the energetics and structures of unsaturated hydrocarbons and, therefore, should not be applied to such systems.

I. INTRODUCTION

The embedded-atom method (EAM), developed by Daw and Baskes^{1,2} in the early 1980s, is a semi-empirical N -body potential useful for the atomistic simulations of metal systems. It has successfully been utilized to calculate the energetics and structures of complex metallic systems involving free surfaces, defects, grain boundaries, etc³. The potential was later modified by Baskes^{4,5} to include the directionality of bonding in covalent materials such as silicon and germanium⁶, leading to the modified embedded-atom method (MEAM)⁵ introduced in 1992. It has undergone several modifications and enhancements since then to include, for example, second nearest-neighbor interactions⁷⁻⁹ and, more recently, a multi-state formalism¹⁰. The unique feature of the MEAM formalism is its ability to reproduce the physical properties of a large number of fcc^{9,11}, bcc^{8,12}, hcp^{13,14}, and diamond cubic¹⁵ crystal structures in unary, binary, ternary, and higher order¹⁶ metal systems with the same semi-empirical formalism. MEAM is also both reliable and transferable¹⁷ in the sense that it accurately reproduces the physical properties of the element or alloy (reliability) and performs reasonably well under circumstances other than the ones used for its parameterization (transferability)¹⁷. Horstemeyer¹⁸ has an excellent review of the MEAM potential in the context of a multi-scale modeling methodology (integrated computational materials engineering) for metals.

The MEAM formalism has traditionally been used for pure metals and impurities, binary and ternary alloys, and carbide, nitride, and hydride metal systems with great success¹⁹. In addition, complex nanostructured systems have been studied using various MEAM-based potentials. For example, Xiao et al.²⁰ calculated the interaction of carbon nanotubes with nickel (Ni) nanoparticles, and Uddin et al.²¹ recently studied the mechanical properties of carbon nanotube-Ni composites using the MEAM potential. We extend the MEAM formalism in the current paper to saturated hydrocarbons with the ultimate aim of capturing the energetics and geometries of commercially important hydrocarbon-based polymers (polyolefins) such as polyethylene and polypropylene. Potentials such as MM3²²⁻²⁴, MM4²⁵, DREIDING²⁶, first-²⁷ and second-generation reactive empirical bond order (REBO)²⁸, reactive force field (ReaxFF)²⁹, charge-optimized many-body (COMB) potential^{30,31}, and condensed-phase optimized molecular potentials for atomistic simulation studies (COMPASS)³² have been used for hydrocarbon simulations, but of these potentials, only REBO, ReaxFF, and COMB are reactive and can allow for bond breaking. Furthermore, most of these potentials are not suitable for hydrocarbon-metal systems, with only ReaxFF³³⁻³⁶ and COMB³⁷ having been used in the past to study hydrocarbon-metal interactions. Liang et al.³⁸ have recently reviewed the use of reactive potentials for advanced atomistic simulations.

In this paper, we develop a new set of parameters within the MEAM framework to describe the interactions and equilibrium geometries of saturated hydrocarbons, specifically bond distances, bond angles, and atomization energies at 0 K. We show that MEAM gives a comparable or more accurate reproduction of these properties relative to experimental and first-principles (FP) data in comparison with REBO and ReaxFF. We also reproduce the potential energy curves of H_2 , CH , and C_2 diatomics and $(\text{H}_2)_2$, $(\text{CH}_4)_2$, $(\text{C}_2\text{H}_6)_2$, and $(\text{C}_3\text{H}_8)_2$ dimer configurations and predict the pressure-volume-temperature (PVT) relationships of a series of select methane, ethane, propane, and butane systems in a reasonable agreement with the experimental data. The energetics of C-H and C-C bond breaking in methane and ethane and the heat of reaction for select chemical reactions are also presented. MEAM gives reasonable predictions of the energies associated with these two major chemical reactions in

saturated hydrocarbons. The development of the first MEAM-based interatomic potential for saturated hydrocarbons and hydrocarbon-based polymers is a step towards reliably simulating systems and phenomena that have hitherto been difficult to study, such as reactive multicomponent (organics/metal) systems, polymer-metal interfaces and nanocomposites, fracture and crack growth in polymers, etc.

This paper is organized in the following manner. In Section II the theory of the MEAM formalism is reviewed. In Section III, the potential development and parameterization is described. The results are given in Section IV.

II. THEORY

In the EAM and MEAM formalisms^{1,2,5} the total energy of a system of like atoms (E_{tot}) is given by

$$E_{tot} = \sum_i \left[F_{\tau_i}(\bar{\rho}_i) + \frac{1}{2} \sum_{j(\neq i)} S_{ij} \phi_{\tau_i \tau_j}(R_{ij}) \right], \quad (1)$$

where F_{τ_i} is the embedding energy function for element type τ_i , which is defined as the energy required to embed an atom of element type τ_i in the background electron density $\bar{\rho}_i$ at site i , S_{ij} is the screening factor between atoms at sites i and j (defined in Eqs. 25 and 28), and $\phi_{\tau_i \tau_j}$ is the pair interaction between atoms of element types τ_i and τ_j at sites i and j at the separation distance of R_{ij} . To emphasize the multi-component nature of the model, the element type of the atom at site i is denoted as τ_i in this manuscript to distinguish it from site designation i , and the screening factor is explicitly separated from the pair potential. The embedding function is given by the specific simple form

$$F_{\tau_i}(\bar{\rho}_i) = \begin{cases} A_{\tau_i} E_{\tau_i}^0 \frac{\bar{\rho}_i}{\bar{\rho}_{\tau_i}^0} \left(\ln \frac{\bar{\rho}_i}{\bar{\rho}_{\tau_i}^0} \right) & \text{if } \bar{\rho}_i \geq 0 \\ -A_{\tau_i} E_{\tau_i}^0 \frac{\bar{\rho}_i}{\bar{\rho}_{\tau_i}^0} & \text{if } \bar{\rho}_i < 0 \end{cases}, \quad (2)$$

where A_{τ_i} is a scaling factor, $E_{\tau_i}^0$ is the sublimation (cohesive) energy, and $\bar{\rho}_{\tau_i}^0$ is the background electron density for the reference structure of the atom of element type τ_i at site i . For most elements, the reference structure is the equilibrium structure of the element in its reference state. However, the reference structure of carbon is taken as diamond. We will denote the properties of the equilibrium reference state with a superscript zero. The analytic continuation of the embedding function for negative electron densities was considered as a computational convenience to prevent systems from entering this unphysical regime. The origin of negative electron densities arises below in Eq. 8. The MEAM formalism introduces directionality in bonding between atoms through decomposing $\bar{\rho}_i$ into spherically symmetric ($\rho_i^{(0)}$) and angular ($\rho_i^{(1)}$, $\rho_i^{(2)}$, and $\rho_i^{(3)}$) partial electron densities^{5,19,39} as given by

$$\rho_i^{(0)} = \sum_{j \neq i} S_{ij} \rho_{\tau_i}^{a(0)}(R_{ij}), \quad (3)$$

$$\left(\rho_i^{(1)}\right)^2 = \frac{\sum_{\alpha} \left[\sum_{j \neq i} \frac{R_{ij}^{\alpha}}{R_{ij}} S_{ij} t_{\tau_j}^{(1)} \rho_{\tau_j}^{a(1)} (R_{ij}) \right]^2 \rho_i^{(0)}}{\sum_{j \neq i} S_{ij} \left(t_{\tau_j}^{(1)} \right)^2 \rho_{\tau_j}^{a(0)} (R_{ij})}, \quad (4)$$

$$\left(\rho_i^{(2)}\right)^2 = \frac{\left\{ \sum_{\alpha, \beta} \left[\sum_{j \neq i} \frac{R_{ij}^{\alpha} R_{ij}^{\beta}}{R_{ij}^2} S_{ij} t_{\tau_j}^{(2)} \rho_{\tau_j}^{a(2)} (R_{ij}) \right]^2 - \frac{1}{3} \left[\sum_{j \neq i} S_{ij} t_{\tau_j}^{(2)} \rho_{\tau_j}^{a(2)} (R_{ij}) \right]^2 \right\} \rho_i^{(0)}}{\sum_{j \neq i} S_{ij} \left(t_{\tau_j}^{(2)} \right)^2 \rho_{\tau_j}^{a(0)} (R_{ij})}, \quad (5)$$

$$\left(\rho_i^{(3)}\right)^2 = \frac{\left\{ \sum_{\alpha, \beta, \gamma} \left[\sum_{j \neq i} \frac{R_{ij}^{\alpha} R_{ij}^{\beta} R_{ij}^{\gamma}}{R_{ij}^3} S_{ij} t_{\tau_j}^{(3)} \rho_{\tau_j}^{a(3)} (R_{ij}) \right]^2 - \frac{3}{5} \sum_{\alpha} \left[\sum_{j \neq i} \frac{R_{ij}^{\alpha}}{R_{ij}} S_{ij} t_{\tau_j}^{(3)} \rho_{\tau_j}^{a(3)} (R_{ij}) \right]^2 \right\} \rho_i^{(0)}}{\sum_{j \neq i} S_{ij} \left(t_{\tau_j}^{(3)} \right)^2 \rho_{\tau_j}^{a(0)} (R_{ij})}. \quad (6)$$

$\rho_{\tau_j}^{a(h)}$ ($h = \{0, 1, 2, 3\}$) indicate the atomic electron densities from atom of element type τ_j at site j at distance R_{ij} from site i . R_{ij}^{α} , R_{ij}^{β} , and R_{ij}^{γ} represent the α , β , and γ components of the distance vector between atoms at sites i and j , respectively, and $t_{\tau_j}^{(h)}$ ($h = \{1, 2, 3\}$) are adjustable element-dependent parameters. The equivalence between these expressions and an expansion in Legendre polynomials has been discussed previously⁵, and $\rho_i^{(h)}$ ($h = \{0, 1, 2, 3\}$) can be thought of as an expansion of the atomic electron density into s , p , d , and f orbital functions. As above, we have carefully denoted the element types of the atoms, and separated the screening from the atomic electron densities. Note that Eq. 3 is the simple linear superposition of atomic densities of the EAM formalism^{1,2}, and Eqs. 4-6 reduce to more familiar forms in the original MEAM paper by Baskes⁵ for a single-component system. The above partial electron densities can be combined in different ways to give the total background electron density at site i ($\bar{\rho}_i$). Here, we adopt one of the most widely used forms^{16,17,40}, which is given by

$$\bar{\rho}_i = \rho_i^{(0)} G(\Gamma_i), \quad (7)$$

$$G(\Gamma_i) = \begin{cases} \sqrt{1 + \Gamma_i} & \text{if } \Gamma_i \geq -1 \\ -\sqrt{|1 + \Gamma_i|} & \text{if } \Gamma_i < -1 \end{cases}, \quad (8)$$

$$\Gamma_i = \sum_{h=1}^3 \bar{t}_i^{(h)} \left[\frac{\rho_i^{(h)}}{\rho_i^{(0)}} \right]^2, \quad (9)$$

$$\bar{t}_i^{(h)} = \frac{1}{\rho_i^{(0)}} \sum_{j \neq i} t_{\tau_j}^{(h)} \rho_{\tau_j}^{a(0)} S_{ij}. \quad (10)$$

In the absence of angular contributions to the density, $\Gamma_i = 0$, $G(\Gamma_i) = 1$, and the model reduces to the EAM formalism. For systems with negative $t_{\tau_j}^{(h)}$ values in certain geometries, $\Gamma_i < -1$, and for computational convenience we perform an analytic continuation of $G(\Gamma_i)$. We choose to do this by allowing $G(\Gamma_i)$ and hence $\bar{\rho}_i$ to become less than zero.

If we apply Eqs. 7 and 9 to the equilibrium reference structure, we obtain

$$\bar{\rho}_{\tau}^0 = Z_{\tau}^0 \rho_{\tau}^0 G(\Gamma_{\tau}^0), \quad (11)$$

$$\Gamma_{\tau}^0 = \sum_{h=1}^3 t_{\tau}^{(h)} s_{\tau}^{(h)} \left(\frac{1}{Z_{\tau}^0} \right)^2, \quad (12)$$

where we have assumed that the reference structure has only first nearest-neighbor interactions. In Eq. 11, ρ_{τ}^0 is an element-dependent electron density scaling factor, and Z_{τ}^0 is the first nearest-neighbor coordination number of the reference structure. $s_{\tau}^{(h)}$ ($h = \{1, 2, 3\}$) are “shape factors” that depend on the reference structure for element type τ . The shape factors are given in the original MEAM paper by Baskes⁵. The atomic electron density for element type τ is calculated from

$$\rho_{\tau}^{a(h)}(R) = \rho_{\tau}^0 e^{-\beta_{\tau}^{(h)} \left(\frac{R}{R_{\tau}^0} - 1 \right)}, \quad (13)$$

where $\beta_{\tau}^{(h)}$ ($h = \{0, 1, 2, 3\}$) are adjustable element-dependent parameters, and R_{τ}^0 is the nearest-neighbor distance in the equilibrium reference structure for the element type τ .

The pair interaction for like atoms of element type τ can be calculated using a first nearest-neighbor (1NN)⁵ or second nearest-neighbor (2NN)^{7,19} formalism. In this work, the former is used^{16,17} and is given by

$$\phi_{\tau\tau}(R) = \frac{2}{Z_{\tau}^0} \{ E_{\tau}^u(R) - F_{\tau}[\bar{\rho}_{\tau}^{ref}(R)] \}. \quad (14)$$

In this equation $\bar{\rho}_{\tau}^{ref}(R)$ is the background electron density in the reference structure evaluated from Eqs. 7-10 at a nearest-neighbor distance of R and is given by

$$\bar{\rho}_{\tau}^{ref}(R) = Z_{\tau}^0 \rho_{\tau}^0 G(\Gamma_{\tau}^{ref}), \quad (15)$$

$$\Gamma_{\tau}^{ref} = \sum_{h=1}^3 t_{\tau}^{(h)} s_{\tau}^{(h)} \left(\frac{\rho_{\tau}^{a(h)}}{Z_{\tau}^0 \rho_{\tau}^{a(0)}} \right)^2, \quad (16)$$

and E_{τ}^u is the universal equation of state (UEOS) of Rose et al.⁴¹ for element type τ given by

$$E_{\tau}^u(R) = -E_{\tau}^0 \left[1 + a^* + \delta \frac{R_{\tau}^0}{R} (a^*)^3 \right] e^{-a^*}, \quad (17)$$

$$a^* = \alpha_{\tau}^0 \left(\frac{R}{R_{\tau}^0} - 1 \right), \quad (18)$$

$$\delta = \begin{cases} \delta_\tau^a & \text{if } a^* \geq 0 \\ \delta_\tau^r & \text{if } a^* < 0 \end{cases}, \quad (19)$$

$$\alpha_\tau^0 = \sqrt{\frac{9K_\tau^0 \Omega_\tau^0}{E_\tau^0}}, \quad (20)$$

or

$$\alpha_\tau^0 = \sqrt{\frac{k_\tau^0}{E_\tau^0}} R_\tau^0. \quad (21)$$

In the above equations K_τ^0 (k_τ^0) and Ω_τ^0 are the bulk modulus (spring constant) and the atomic volume of the reference structure, respectively, and δ is an adjustable, element-dependent parameter that has two components, attractive δ_τ^a and repulsive δ_τ^r . Eq. 20 is used when the reference structure is a three-dimensional (3D) crystal and Eq. 21 is used when the reference structure is a diatomic.

The pair interaction for unlike atoms of element types τ and v is similarly obtained from the reference structure of the unlike atoms. For this work, the reference structure is taken as the heteronuclear diatomic, which gives

$$\phi_{\tau v}(R) = \frac{1}{Z_{\tau v}^0} \{ 2E_{\tau v}^u(R) - F_\tau [\bar{\rho}_v^d(R)] - F_v [\bar{\rho}_\tau^d(R)] \}, \quad (22)$$

where $Z_{\tau v}^0 = 1$ is the coordination number for the diatomic and

$$\bar{\rho}_\tau^d(R) = \rho_\tau^{a(0)} G(\Gamma_\tau^d), \quad (23)$$

$$\Gamma_\tau^d = \sum_{h=1}^3 t_\tau^{(h)} s_d^{(h)} \left(\frac{\rho_\tau^{a(h)}}{\rho_\tau^{a(0)}} \right)^2, \quad (24)$$

where the shape factors $s_d^{(h)}$ are those for a diatomic. The UEOS $E_{\tau v}^u$ is given by Eqs. 17-21 using parameters $E_{\tau v}^0$, $R_{\tau v}^0$, $k_{\tau v}^0$, $\delta_{\tau v}^a$, and $\delta_{\tau v}^r$.

The screening factor S_{ij} is defined as the product of all screening factors S_{ikj} , where the interaction between atoms at sites i and j are screened by neighboring atoms at site k as given by

$$S_{ij} = \prod_{k \neq i,j} S_{ikj}. \quad (25)$$

If it is assumed that all three sites i , j , and k lie on an ellipse on the xy -plane with sites i and j on the x-axis, the following equation can be derived:

$$x^2 + \frac{1}{C} y^2 = \left(\frac{1}{2} R_{ij} \right)^2, \quad (26)$$

where

$$C_{ikj} = \frac{2(X_{ik} + X_{kj}) - (X_{ik} - X_{kj})^2 - 1}{1 - (X_{ik} - X_{kj})^2}. \quad (27)$$

In the above equation $X_{ik} = (R_{ik}/R_{ij})^2$ and $X_{kj} = (R_{kj}/R_{ij})^2$. The screening factor S_{ikj} for like atoms is defined as

$$S_{ikj} = f_c \left(\frac{C_{ikj} - C_{min}(\tau_i, \tau_k, \tau_j)}{C_{max}(\tau_i, \tau_k, \tau_j) - C_{min}(\tau_i, \tau_k, \tau_j)} \right), \quad (28)$$

where $C_{min}(\tau_i, \tau_k, \tau_j)$ and $C_{max}(\tau_i, \tau_k, \tau_j)$ determine the extent of screening of atoms of element type τ at sites i and j by an atom at site k . Similar expressions can be written for the screening of unlike atoms. The smooth cutoff function f_c is defined as

$$f_c(x) = \begin{cases} 1 & \text{if } x \geq 1 \\ [1 - (1 - x)^4]^2 & \text{if } 0 < x < 1 \\ 0 & \text{if } x \leq 0 \end{cases}. \quad (29)$$

$S_{ij} = 1$ means that the interaction between atoms at sites i and j is not screened, while $S_{ij} = 0$ means the interaction is completely screened.

III. POTENTIAL PARAMETERIZATION

The MEAM formalism presented in Eqs. 1-29 requires 16 independent model parameters for each element type τ , *i.e.*, E_τ^0 , R_τ^0 , α_τ^0 , δ_τ^a , and δ_τ^r for the universal equation of state (Eq. 17); $\beta_\tau^{(0)}$, $\beta_\tau^{(1)}$, $\beta_\tau^{(2)}$, $\beta_\tau^{(3)}$, $t_\tau^{(1)}$, $t_\tau^{(2)}$, $t_\tau^{(3)}$, and ρ_τ^0 for the electron densities (Eqs. 3-13); A_τ for the embedding function F_τ (Eq. 2); and C_{min} and C_{max} for the screening factor (Eqs. 25-29). In the current MEAM formalism for a single element, model is independent of ρ_τ^0 ; hence, $\rho_\tau^0 = 1$ is taken for one of the elements. For a diatomic composed of elements τ and ν , 13 additional independent parameters are required, *i.e.*, $E_{\tau\nu}^0$, $R_{\tau\nu}^0$, $\alpha_{\tau\nu}^0$, $\delta_{\tau\nu}^a$, and $\delta_{\tau\nu}^r$, four C_{min} , and four C_{max} values.

In this work, we parameterized the elements carbon and hydrogen and the diatomic CH with the reference structures of diamond for carbon ($Z_C^0 = 4$), diatomic H₂ for hydrogen ($Z_H^0 = 1$), and diatomic CH for hydrocarbons ($Z_{CH}^0 = 1$). As initial starting parameters for this potential, we utilized the MEAM parameters for carbon from the work of Xiao et al.²⁰ and the parameters for hydrogen from the work of Baskes⁵. The fitting procedure for the pure element parameters is described in detail by Baskes⁵. For the potential parameterization, we utilized a parameter fitting database consisting of 1) experimental bond distances⁴², bond angles⁴², and atomization energies at 0 K of a homologous series of alkanes and their isomers from methane to *n*-octane^{43,44} 2) potential energy curves of H₂, C₂, and CH diatomics, generated in this work from FP calculations, 3) FP interaction energy curves of (H₂)₂ (H₂ dimer)⁴⁵, (CH₄)₂ (methane dimer)⁴⁶, (C₂H₆)₂ (ethane dimer)⁴⁷, and (C₃H₈)₂ (propane dimer)⁴⁸ in select molecular orientations, and 4) the pressure-volume-temperature (*PVT*) experimental data for a dense methane system⁴⁹. The FP data for H₂, C₂, and CH diatomics were generated with the CCSD(2)⁵⁰ ab initio method and the aug-cc-pVTZ basis set⁵¹ using Q-Chem® quantum chemistry software (V3.2)⁵² and restricted core orbitals. CCSD(2) is a high-accuracy FP method designed to calculate bond breaking with great

precision⁵³. The MEAM fitting procedure involved a stepwise and iterative effort to first capture the energy versus distance characteristics of the H₂, CH, and C₂ diatomics. Next, we fit the atomization energies of the linear alkanes to the experimental data that were first corrected for the zero-point energy (ZPE). The bond distances and bond angles of the first four alkanes and one butane isomer were then fit to the experimental data. To enable a reliable prediction of the van der Waals forces, we further fit the MEAM parameters to the interaction energy curves of (H₂)₂, (CH₄)₂, (C₂H₆)₂, and (C₃H₈)₂ dimers, which we validated in subsequent molecular dynamics (MD) simulations of lower alkane systems to establish *PVT* relationships. This collective fitting to the FP dimer interactions was made in conjunction with the prediction of the experimental *PVT* behavior of a dense high-pressure methane system (density of 0.5534 g/cc). The FP data for the dimer interactions were taken from literature values, some of which are quite dated. However, since these dimer interactions were merely used as guidance to tune in the actual pressure values of the methane system at a given density and temperature, the comparisons of MEAM predictions with the FP data (see Section IV) should only be construed as qualitative. The *PVT* validations with the experimental data, together with the MEAM predictions for the bond distances, bond angles, dihedral (torsion) angles, and atomization energies of a series of alkanes and free radicals as well as the energetics of C-H and C-C bond breaking and heat of reaction for a few select reactions, are given in Section IV. During the parameterization process, we found the value of the α_H^0 parameter in the work of Baskes⁵ to be incorrect due to an error in the implementation of the equation for the diatomic force constant of the H-H bond. The value of this parameter was corrected in the present work, and the corrected value appears in Table I. The final sets of MEAM parameters for carbon, hydrogen, and CH is given in Tables I and II.

IV. RESULTS

A. Single Molecules

The MEAM atomization energies of select alkanes, free radicals, and unsaturated compounds (for illustration purposes) are given in Table III. In the same table, the experimental atomization energies at 0 K^{43,44} are also given, along with the values calculated using the REBO and ReaxFF potentials. The starting molecular structures were created in the Avogadro open-source molecular builder and visualization tool⁵⁴ and initially optimized using Avogadro's built-in Molecular Merck Force Field (MMFF94)⁵⁵. The energies of the resulting structures were then minimized using MEAM, REBO, and ReaxFF potentials and the Polak-Ribiere conjugate gradient method⁵⁶. We utilized the parameters for carbon and hydrogen in the second-generation REBO and ReaxFF from the work of Brenner et al.²⁸ and Mattsson et al.⁵⁷, respectively. The REBO and ReaxFF calculations were performed on the open-source large-scale atomic/molecular massively parallel simulator (LAMMPS) software package⁵⁸ developed at Sandia National Laboratories (version April 20, 2012). The ReaxFF implementation in LAMMPS is based on the formalism introduced by Chenoweth, et al.,⁵⁹ in 2008. This implementation has been validated against the original ReaxFF serial codes.⁵⁷ To further validate the LAMMPS implementation of the ReaxFF code for the purpose of this work, we performed a representative calculation of the ethane rotational barrier using the original parameters of Chenoweth, et al.⁵⁹ embedded in the LAMMPS software package⁵⁸ and compared the results to those published by Chenoweth, et al.⁵⁹ We used the ReaxFF-

TABLE I: Single element MEAM parameters for carbon and hydrogen with diamond and diatomic H_2 reference structures, respectively. E_τ^0 (eV) is the cohesive energy, R_τ^0 (\AA) is the nearest neighbor distance in the equilibrium reference structure, α_τ^0 is the exponential decay factor for the universal energy of Rose et al. 41, A_τ is the electron density scaling factor for the embedding function, ρ_τ^0 is the electron density scaling factor, δ_τ^a and δ_τ^r are the attraction ($a^* \leq 0$) and repulsion ($a^* > 0$) cubic terms for the universal equation of state, $\beta_\tau^{(0-3)}$ are the exponential decay factors for the atomic electron densities, $t_\tau^{(1-3)}$ are the weighting parameters for the atomic electron densities, and C_{min} and C_{max} are the screening parameters for three like atoms of the element τ .

Element	E_τ^0	R_τ^0	α_τ^0	A_τ	ρ_τ^0	δ_τ^a	δ_τ^r	$\beta_\tau^{(1)}$	$\beta_\tau^{(2)}$	$\beta_\tau^{(3)}$	$t_\tau^{(1)}$	$t_\tau^{(2)}$	$t_\tau^{(3)}$	C_{min}	C_{max}	
C	7.370	1.44	3.60	0.64	1.00	0.00	0.00	4.20	4.50	4.30	4.18	0.50	0.45	-3.80	2.00	2.80
H	2.363	0.74	2.0388	2.50	1.80	0.00	0.05	2.72	2.045	2.25	-	0.20	-0.40	0.00	0.75	2.80

TABLE II: MEAM interaction and screening parameters for the diatomic C-H. R_{CH}^0 (Å) is the first nearest neighbor distance, α_{CH}^0 is the exponential decay factor for the universal equation of state (UEOS) of Rose et al.⁴¹, E_{CH}^0 (eV) is the cohesive energy, δ_{CH}^a and δ_{CH}^r are the attraction ($a^* > 0$) and repulsion ($a^* \leq 0$) cubic terms for the UEOS, respectively, and C_{min} and C_{max} are the parameters for the screening factor. The middle atom screens the other two atoms (see Section II).

Parameter	Value
R_{CH}^0	1.02
α_{CH}^0	3.20
E_{CH}^0	2.12
δ_{CH}^a	0.05
δ_{CH}^r	0.05
$C_{min}(C, C, H)$	0.445
$C_{max}(C, C, H)$	2.80
$C_{min}(C, H, C)$	2.00
$C_{max}(C, H, C)$	2.80
$C_{min}(C, H, H)$	1.50
$C_{max}(C, H, H)$	2.00
$C_{min}(H, C, H)$	0.52
$C_{max}(H, C, H)$	2.20

minimized ethane structure as the initial geometry since this information was not disclosed by Chenoweth and co-workers. The LAMMPS-calculated relative energies of the 0°, 30°, and 60° H-C-C-H dihedral angles for ethane were 3.57, 1.78, and 0 kcal/mol, respectively. The energies for the dihedral angles reported by Chenoweth, et al.⁵⁹ were 3.42, 1.61, and 0 kcal/mol, respectively. The 0.15 kcal/mol difference in these values is acceptable given the initial geometries may not be the same. We take these calculations as validation for the LAMMPS implementation of ReaxFF, but use the newer ReaxFF parameters by Mattsson, et al.⁵⁷ in this work. The REBO implementation in LAMMPS was directly verified by comparing the LAMMPS-calculated energies of the molecular structures in Table III with those published by Brenner, et al.²⁸.

All MEAM calculations and simulations were performed on DYNAMO software (V8.7), developed by Foiles, Daw, and Baskes⁶⁰ at Sandia National Laboratories. The MEAM potential was fit to the experimental data corrected for ZPE. Hence, the corrected value in Table III should be compared with the experimental data. Similarly, in the second generation REBO, a ZPE correction needs to be applied to the LAMMPS calculated energies of hydrocarbon structures²⁸. The reported atomization energies in Table III reflect these corrections based on the ZPE data reported by Brenner et al.²⁸ and B3LYP/6-31G** density functional theory (DFT) ZPE calculations performed as part of this work. Furthermore, since ReaxFF was fit to the heats of formation of hydrocarbons²⁹, it is necessary to correct the LAMMPS-calculated energies by the empirical “heat increments” discussed in the work of van Duin et al.²⁹. We corrected the LAMMPS-calculated energies for the structures using the ReaxFF potential by calculating the differences between the ReaxFF empirical heat increments for carbon (9.489 eV) and hydrogen (2.355 eV)²⁹ and the experimental energies

for carbon (7.3768 eV) and hydrogen (2.375 eV)²⁷, and then subtracting the total difference for carbon and hydrogen atoms in the molecules from the LAMMPS-calculated energies. The root-mean-square (RMS) error associated with the MEAM-reproduced atomization energies of the alkanes in Table III (0.19 eV) compares well with that of REBO (0.11 eV) and is far better than that of ReaxFF (0.99 eV). The systems with the largest errors for MEAM contain double and triple bonds. This is not surprising since MEAM is not parameterized for these systems. However, MEAM does give a reasonable prediction of the atomization energies of methyl (CH_3), ethyl ($\text{H}_3\text{C}_2\text{H}_2$), and isopropyl (CH_3CHCH_3) radicals, which are representative molecular fragments for the bond-breaking reactions that can occur in saturated hydrocarbons. A comparison between the atomization energies relative to the experimental data for the three potentials is given in Fig. 1. Of course, REBO and ReaxFF have been parameterized to a larger database of both saturated and unsaturated hydrocarbons, and therefore, they can be applied to a much larger range of systems. Hence, the comparisons in Table III serve only as a guide.

The average equilibrium bond distances and bond angles for the first three molecules in the alkane series and both isomers of butane are given in Tables IV and V, respectively, where the MEAM, REBO, and ReaxFF values are compared to the experimental data⁴². The MEAM results give lower RMS errors for both bond distances and bond angles than REBO or ReaxFF. In Figs. 2 and 3, the bond distances and bond angles relative to the experimental data are depicted for the three potentials.

In Table VI, the MEAM-predicted dihedral (torsion) angle for the gauche conformer of isobutane is compared to the predictions by REBO and ReaxFF as well as the experimental data. MEAM reproduces the angle within 20% of the experimental value, while REBO and ReaxFF reproduce it within 5% and 3%, respectively.

To validate whether the MEAM potential correctly predicts the formation of molecular species with expected geometries after energy minimization, two atomic configurations were selected and energy-minimized: 1) CH_3 in non-planar configuration with an initial $\angle\text{H-C-H}$ of 109.5° (to validate the formation of planar structure after energy minimization and a final $\angle\text{H-C-H}$ of 120°), and 2) CH_4+2H with the two extra hydrogen atoms on either side of the methane molecule and very close to it (to validate the repulsion of the two extra hydrogen atoms and formation of a hydrogen molecule away from the methane molecule). Correct prediction of the resulting molecular species and their geometries is crucial for reliably simulating reactions involving free radicals. MEAM and REBO both predicted a planar CH_3 structure with a final $\angle\text{H-C-H}$ of 120° after energy minimization, while ReaxFF gave a slightly non-planar structure with a final $\angle\text{H-C-H}$ of 117.4°. Furthermore, for the CH_4+2H structure, both MEAM and REBO predicted the formation of a hydrogen molecule away from an equilibrated methane molecule, while ReaxFF minimized the structure to a non-equilibrium configuration. The initial and final structures for the CH_4+2H atomic configuration calculated by MEAM, REBO, and ReaxFF are given in Fig. 4.

TABLE III: Atomization energies of a homologous series of alkanes from methane to *n*-octane and their select isomers, cycloalkanes, free radicals, hydrogen, and carbon diatomic reproduced by MEAM, REBO, and ReaxFF potentials versus experimental data.

Molecule	Atomization energy at 0 K (eV)							
	Expt. ^b	ZPE ^d	MEAM ⁵		REBO ²⁸		ReaxFF ²⁹	
			DYNAMO	Corr. ^f	LAMMPS ^g	Corr. ^h	LAMMPS ⁱ	Corr. ^j
H ₂	4.478	0.263 ^e	4.726	4.463	4.506	4.243	4.804	4.845
C ₂	6.219	0.111 ^e	5.804	5.693	6.21	6.099	10.902	6.697
<u>Alkanes</u>								
methane	17.018	1.135	18.319	17.184	18.185	17.05	19.202	17.181
ethane	28.885	1.921	30.991	29.07	30.846	28.925	33.279	29.196
propane	40.88	2.706	43.658	40.952	43.589	40.883	47.64	41.495
<i>n</i> -butane	52.896	3.492	56.322	52.83	56.332	52.84	61.921	53.714
isobutane	52.977	3.492	56.377	52.885	56.331	52.839	62.063	53.856
<i>n</i> -pentane	64.915	4.278	68.985	64.707	69.076	64.798	76.022	65.753
isopentane	64.964	4.278	69.107	64.829	69.073	64.795	76.26	65.991
neopentane	65.123	4.278	69.177	64.899	69.061	64.783	76.614	66.345
<i>n</i> -hexane	76.922	4.892 ^e	81.648	76.756	81.819	76.929	90.204	77.873
iso hexane	76.975	4.896 ^e	81.68	76.784	81.817	76.921	90.259	77.928
3-methylpentane	76.946	4.885 ^e	81.712	76.827	81.817	76.932	90.312	77.981
2,3-dimethylbutane	76.97	4.867 ^e	81.73	76.863	81.815	76.948	90.467	78.136
neohexane	77.06	4.876e	81.772	76.896	81.804	76.928	90.721	78.39
<i>n</i> -heptane	88.957^c	5.623 ^e	94.311	88.688	94.562	88.939	104.489	90.096
isoheptane	89.008^c	5.622 ^e	94.346	88.724	94.56	88.938	104.652	90.259
<i>n</i> -octane	100.971^c	6.359 ^e	106.975	100.616	107.306	100.947	118.692	102.237
RMS Error ^a :	-	-	-	0.19	-	0.11	-	0.99
<u>Alkenes</u>								
ethene (ethylene)	23.066	1.303	22.955	21.652	24.528	23.225	27.183	23.059
<u>Alkynes</u>								
ethyne (acetylene)	16.857	0.686	14.552	13.866	17.565	16.879	19.952	15.7874
<u>Cycloalkanes</u>								
cyclopropane	34.818	2.089	37.636	35.547	36.889	34.8	41.27	35.084
cyclobutane	46.848	2.875	50.441	47.566	49.898	47.023	54.402	46.154
cyclopentane	59.707	3.66	63.252	59.592	63.643	59.983	70.197	59.887
cyclohexane	71.963	4.446	76.059	71.613	76.46	72.014	84.901	72.529
RMS Error ^a :	-	-	-	0.54	-	0.17	-	0.48
<u>Aromatics</u>								
benzene	56.62	2.594	52.308	49.714	60.231	57.637	68.236	55.742
<u>Radicals</u>								
CH	3.469	0.165 ^e	5.493	5.328	4.526	4.361	5.029	2.947
CH ₂	7.41	0.517	10.027	9.51	8.469	7.952	9.766	7.704
CH ₃	12.534	0.826	14.265	13.439	13.375	12.549	14.806	12.764
C ₂ H	11.125	0.377	10.149	9.772	11.572	11.195	14.897	10.712
H ₃ C ₂ H ₂	24.572	1.612	26.967	25.355	26.588	24.976	29.012	24.908
CH ₃ CHCH ₃	36.676	2.405	39.672	37.267	39.554	37.148	43.027	36.861

^a Root-Mean-Square Error.

^b From the NIST Computational Chemistry Comparison and Benchmark Database⁴³.

^c From Karton et al.⁴⁴

^d Zero-point energies are taken from Brenner et al.²⁸ if not indicated otherwise.

^e B3LYP/6-31G** ZPEs with a scaling factor of 0.95 applied to account for method limitations and anharmonicity.

^f Corrections were made by subtracting the zero-point energies from the DYNAMO⁶⁰ calculated energies.

^g C and H parameters in LAMMPS⁵⁸ (version April 20, 2012) were taken from Brenner et al.²⁸

^h Corrections were made by subtracting the zero-point energies from the LAMMPS⁵⁸ calculated energies.

ⁱ C and H parameters in LAMMPS⁵⁸ (version April 20, 2012) were taken from Mattsson et al.⁵⁷

^j Corrections were made by calculating the differences in the “heat increments” for carbon (9.489 eV) and hydrogen (2.355 eV), as described in the work of van Duin et al.²⁹ from the experimental energies for carbon (7.3768 eV) and hydrogen (2.375 eV), as reported by Brenner et al.²⁷, respectively, and then subtracting the total difference for carbon and hydrogen atoms in the molecules from the LAMMPS⁵⁸ calculated energies.

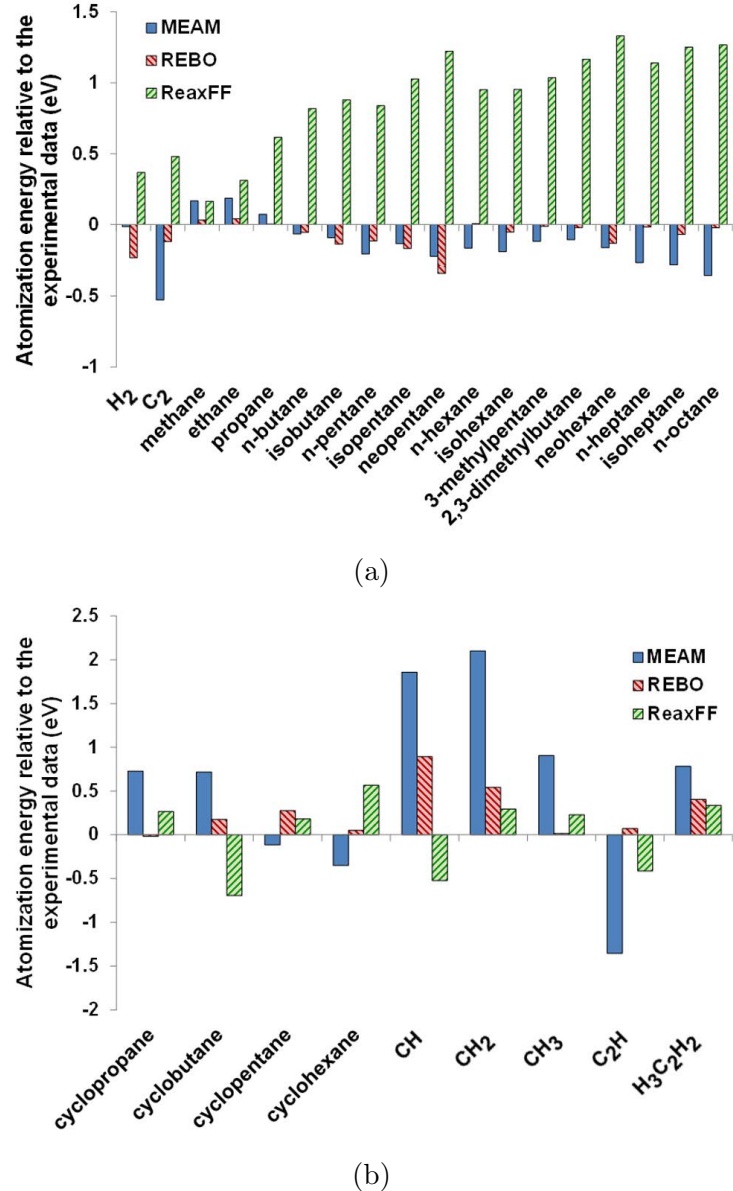


FIG. 1: Errors associated with the corrected MEAM, REBO, and ReaxFF atomization energies of a) hydrogen and linear alkanes and b) cycloalkanes and free radicals relative to the experimental data. The actual data are given in Table III.

TABLE IV: Average equilibrium C-H and C-C bond distances for select alkanes after energy minimization of the molecular structures using the MEAM, REBO, and ReaxFF potentials. The results are compared to the experimental data⁴².

Molecule	Bond distance (Å)							
	C-H				C-C			
	Expt. ^a	MEAM	REBO	ReaxFF	Expt. ^a	MEAM	REBO	ReaxFF
methane	1.087	1.089	1.089	1.118	-	-	-	-
ethane	1.094	1.092	1.090	1.090	1.535	1.534	1.543	1.534
propane	1.107	1.093	1.090	1.110	1.532	1.533	1.542	1.542
<i>n</i> -butane	1.117	1.094	1.090	1.110	1.531	1.533	1.542	1.556
isobutane	1.113	1.094	1.090	1.112	1.535	1.525	1.543	1.545
RMS Error ^b	-	0.015	0.018	0.019	-	0.005	0.009	0.036

^a From Lide⁴².

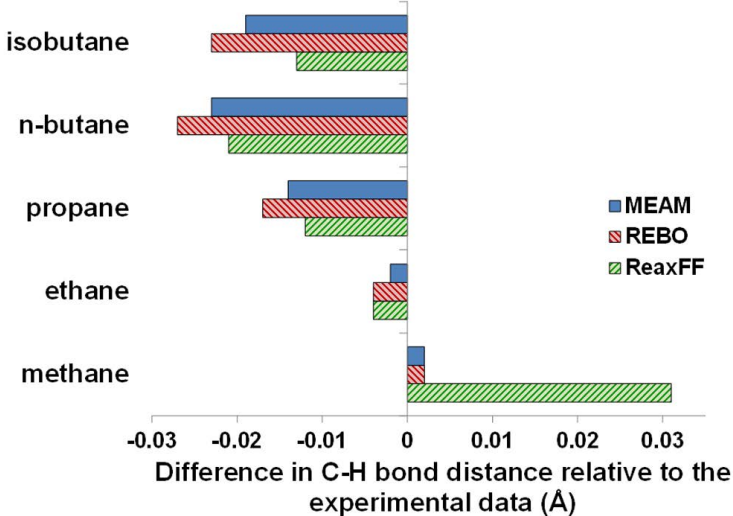
^b Root-Mean-Square Error.

TABLE V: Average equilibrium $\angle\text{H-C-H}$, $\angle\text{H-C-C}$, and $\angle\text{C-C-C}$ bond angles for select alkanes after energy minimization of the molecular structures using the MEAM, REBO, and ReaxFF potentials. The results are compared to the experimental data⁴².

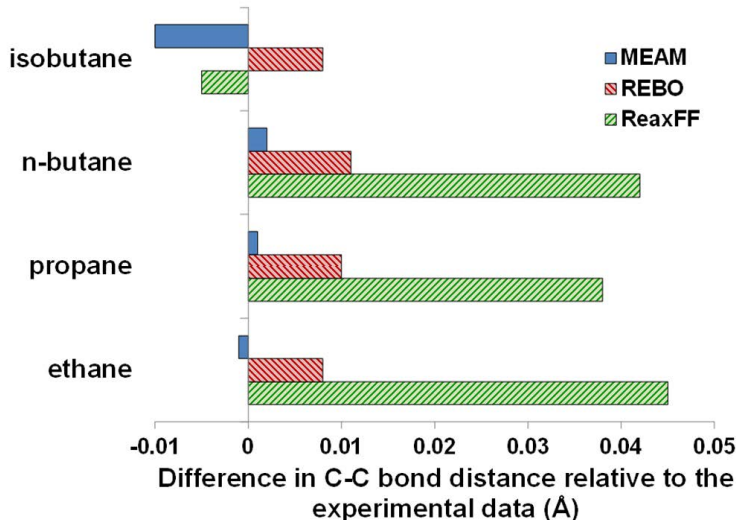
Molecule	$\angle\text{H-C-H}$				$\angle\text{H-C-C}$				Bond angle (°)				$\angle\text{C-C-C}$			
	Expt. ^a	MEAM	REBO	ReaxFF	Expt. ^a	MEAM	REBO	ReaxFF	Expt. ^a	MEAM	REBO	ReaxFF	Expt. ^a	MEAM	REBO	ReaxFF
methane	109.47	109.47	109.47	109.47	-	-	-	-	-	-	-	-	-	-	-	-
ethane	107.70	107.70	108.54	107.30	111.17	111.18	110.39	111.58	-	-	-	-	-	-	-	-
propane	107.00	107.40	108.35	107.00	N/A	110.90	110.20	110.91	111.70	111.80	111.07	111.40	-	-	-	-
<i>n</i> -butane	N/A	107.50	108.22	106.89	111.00	110.60	110.08	110.80	113.80	112.10	111.08	110.90	-	-	-	-
isobutane	N/A	107.40	108.54	107.90	111.40	111.20	110.39	110.70	110.80	109.70	110.23	110.02	-	-	-	-
RMS Error ^b	-	0.23	0.92	0.23	-	0.26	0.91	0.48	-	1.17	1.65	1.74	-	-	-	-

^a From Lide⁴².

^b Root-Mean-Square Error.



(a)



(b)

FIG. 2: Errors associated with the MEAM-, REBO-, and ReaxFF-reproduced bond distances for the a) C-H and b) C-C bonds of select alkanes relative to the experimental data. The actual data are given in Table IV.

TABLE VI: Equilibrium dihedral angle for the gauche conformer of isobutane after energy minimization of the molecular structure using the MEAM, REBO, and ReaxFF potentials. The results are compared to the experimental data⁴².

Expt. ^a	Dihedral angle (°)		
	MEAM	REBO	ReaxFF
65	78	68	67

^a From Lide⁴².

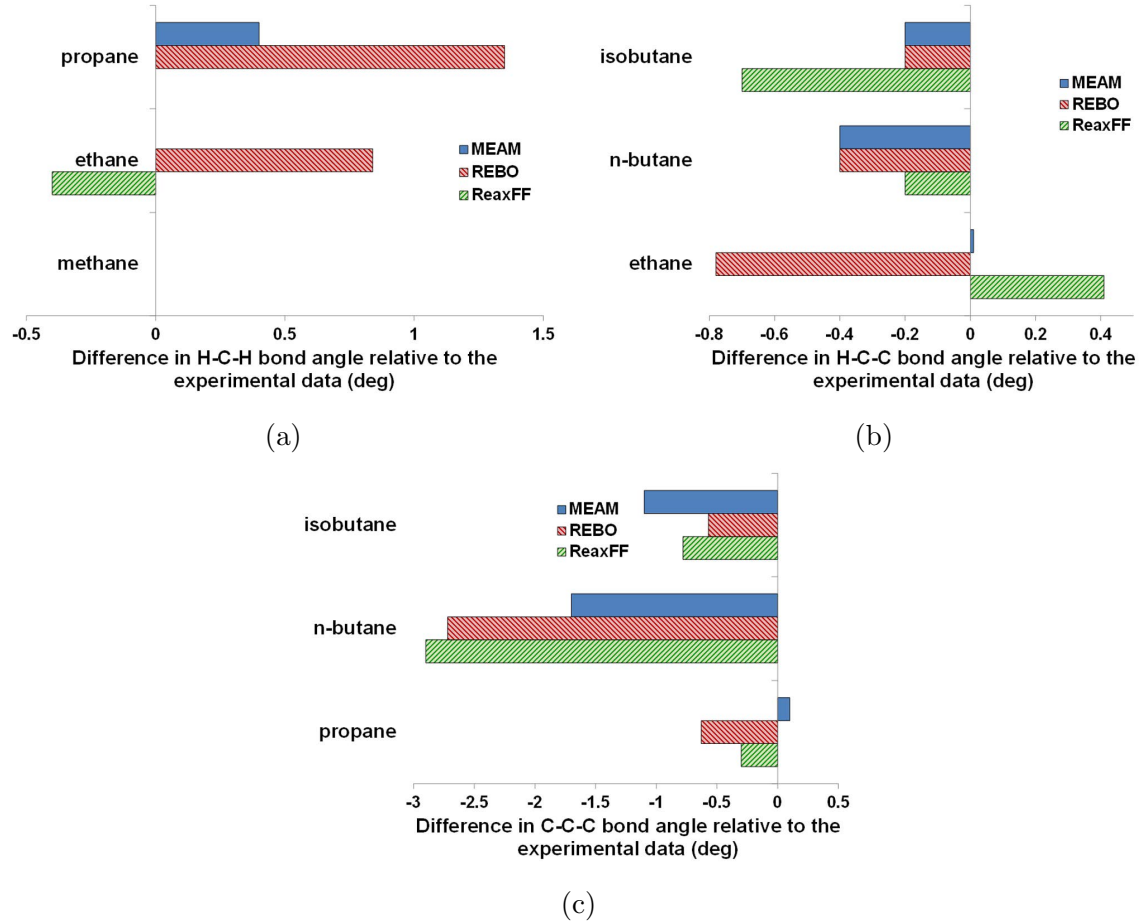


FIG. 3: Errors associated with the MEAM-, REBO-, and ReaxFF-reproduced bond angles for the a) \angle H-C-H, b) \angle H-C-C, and c) \angle C-C-C angles relative to the experimental data. The actual data are given in Table V.

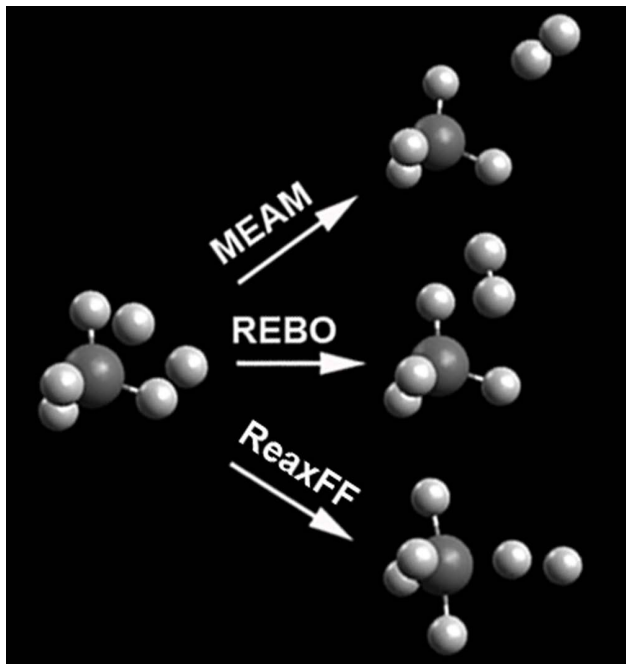


FIG. 4: Initial and final structures of $\text{CH}_4 + 2\text{H}$ atomic configuration resulting from the energy minimization of the structure using the MEAM, REBO, and ReaxFF potentials.

B. Diatomic molecules

The potential energy curves for H_2 , CH , and C_2 diatomics generated by the MEAM, REBO, and ReaxFF potentials are presented in Fig. 5. As stated in Section III, the FP data were generated in this work using CCSD(2) and the aug-cc-pVTZ basis set, and MEAM was fitted to these potential energy curves. The ReaxFF potential implementation in LAMMPS⁵⁸ gives a non-zero energy value for a single carbon atom, $E = -0.075568$ eV. The ReaxFF interaction curves for CH and C_2 were corrected for this non-zero energy associated with the isolated carbon atom at infinite interatomic distances.

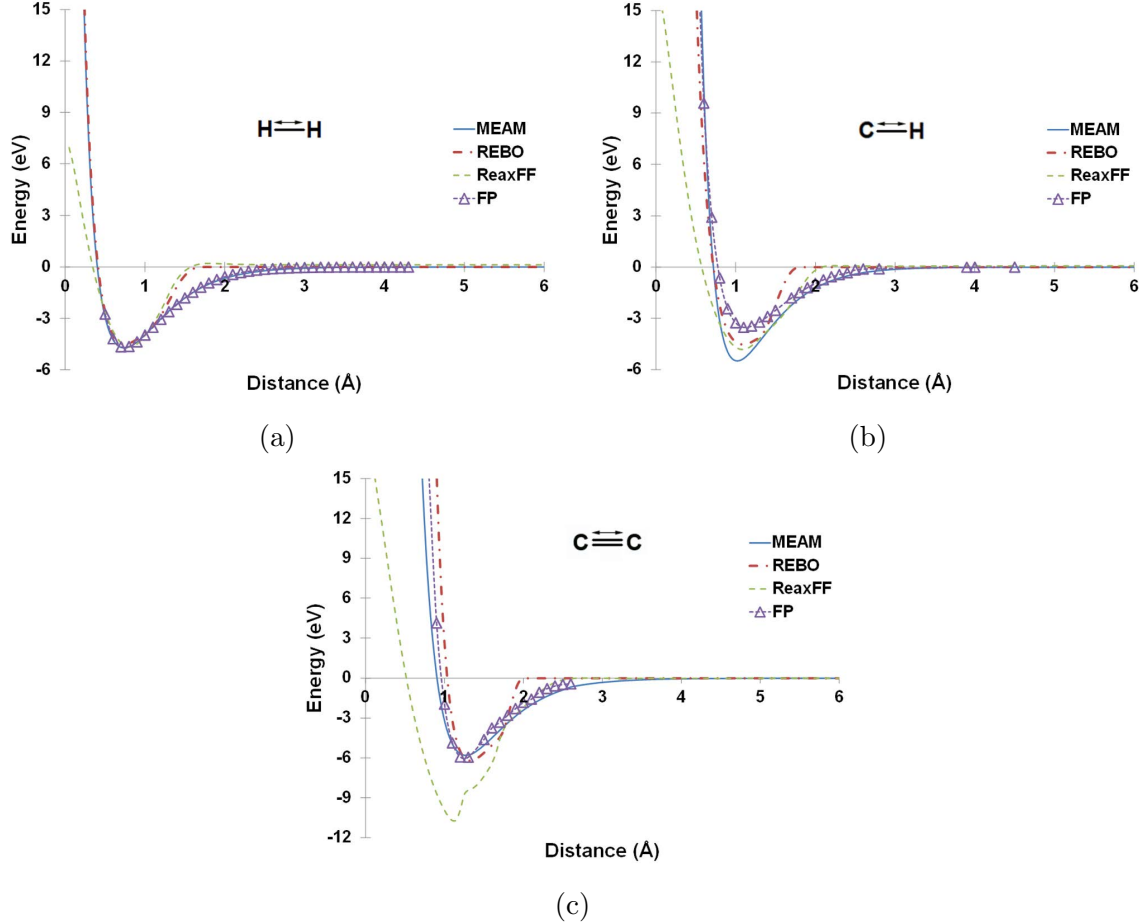


FIG. 5: Potential energy curves of a) H_2 , b) CH , and c) C_2 diatomics. The MEAM results are compared to those of REBO, ReaxFF, and the CCSD(2)/aug-cc-pVTZ FP data generated in this work.

C. Dimer molecules

To reproduce the van der Waals interactions between the molecules, we used the FP interaction energy curves of hydrogen, methane, ethane, and propane dimers in the fitting database (see Section III). The MEAM-reproduced interaction curves are plotted for the five dimers in select molecular orientations versus the FP data in Figs. 6-9. All atoms were

constrained at each distance increment, and the energy was calculated by subtracting the total energy of the structure at infinite atomic distance from the actual energy at each distance increment. The FP data for the hydrogen dimer were taken from the work of Burton et al.⁴⁵, where four different molecular configurations, denoted as collinear coplanar (T), linear (L), parallel or rectangular (P), and crossed or elongated tetrahedron (C), were considered. The configurations are depicted in Fig. 6. The FP data for methane and ethane dimers were taken from the work of Szczesniak et al.⁴⁶ and Rowley and Yang⁴⁷, respectively. In the former, four molecular configurations designated in their work as A, B, D, and F were considered ($R_{CH} = 1.091 \text{ \AA}$). These configurations are depicted in Fig. 7. In the latter, only the first four configurations out of 22 reported in the work of Rowley and Yang, designated as routes 1-4, were used for fitting purposes⁴⁷ ($R_{CH} = 1.102 \text{ \AA}$, $R_{CC} = 1.523 \text{ \AA}$). These routes are given as insets in Fig. 8. The FP data for propane dimer were taken from the work of Jalkanen et al.⁴⁸ with three molecular orientations, designated as bb-ccccc90, bb-bb 90, and ccs-ccs 90, used for fitting purposes ($R_{CH} = 1.102 \text{ \AA}$, $R_{CC} = 1.529 \text{ \AA}$). For details on these orientations and the relevant coding of them, refer to Jalkanen et al.⁴⁸. MEAM reproduces the general trends of the van der Waals bonding. Note that no additional van der Waals term is added to the MEAM formalism presented in Section II. The van der Waals interactions arise directly from the tails of the electron densities and the pair potentials.

D. Bond dissociation reactions and rotational barrier

The MEAM-reproduced C-H and C-C bond dissociation energy curves in methane and ethane and the associated FP data are shown in Figs. 10a and 10b, respectively. The FP curve for the C-H dissociation in methane was generated in this work, while the FP data for the C-C bond dissociation in ethane was taken from the work of Lorant et al.⁶¹. The separating carbon and hydrogen atoms in methane and the two carbon atoms in ethane were constrained, while the structure was minimized at each distance increment. For the FP data of the C-H dissociation, the constrained geometries were minimized with CCSD(T)/aug-cc-pVTZ, and single point energies were calculated with CCSD(2)/aug-cc-pVTZ basis set. The MEAM-generated data show reasonable agreement with the FP results, especially at longer bond distances. To further validate the dissociating geometry of the ethane molecule, the intermediate MEAM-calculated \angle H-C-C bond angles are compared to the FP data⁶¹ in Fig. 11. The general trend of the FP dissociation curves (Fig. 10) is qualitatively captured by MEAM, while the angles at intermediate distances deviates some from FP calculations. However, the beginning and end states of the dissociated molecule have the correct \angle H-C-C bond angles at similar C-C dissociation distances. In systems consisting purely of saturated hydrocarbons, C-H and C-C bond dissociations are the only reactions possible. The heat of reaction data calculated by the MEAM, REBO, and ReaxFF potentials as well as the experimental data for few chemical reactions in saturated hydrocarbons are given in Table VII. In this table, ReaxFF gives the least RMS error (0.20 eV) followed by REBO (0.46 eV) and MEAM (1.23 eV). The results in Figs. 10-11 and Table VII in combination with data given in Table III give confidence that MEAM is suitable for describing the structures, energetics, and reactions of saturated hydrocarbon systems.

The MEAM-calculated rotational barrier for ethane, ethylene and the associated FP data are given in Fig. 12. The FP data calculations are described above. We have calculated the rotational barrier in ethylene in this work, but obtained a barrier of essentially zero. Modification of the model to properly reproduce rotation around double bonds is a subject

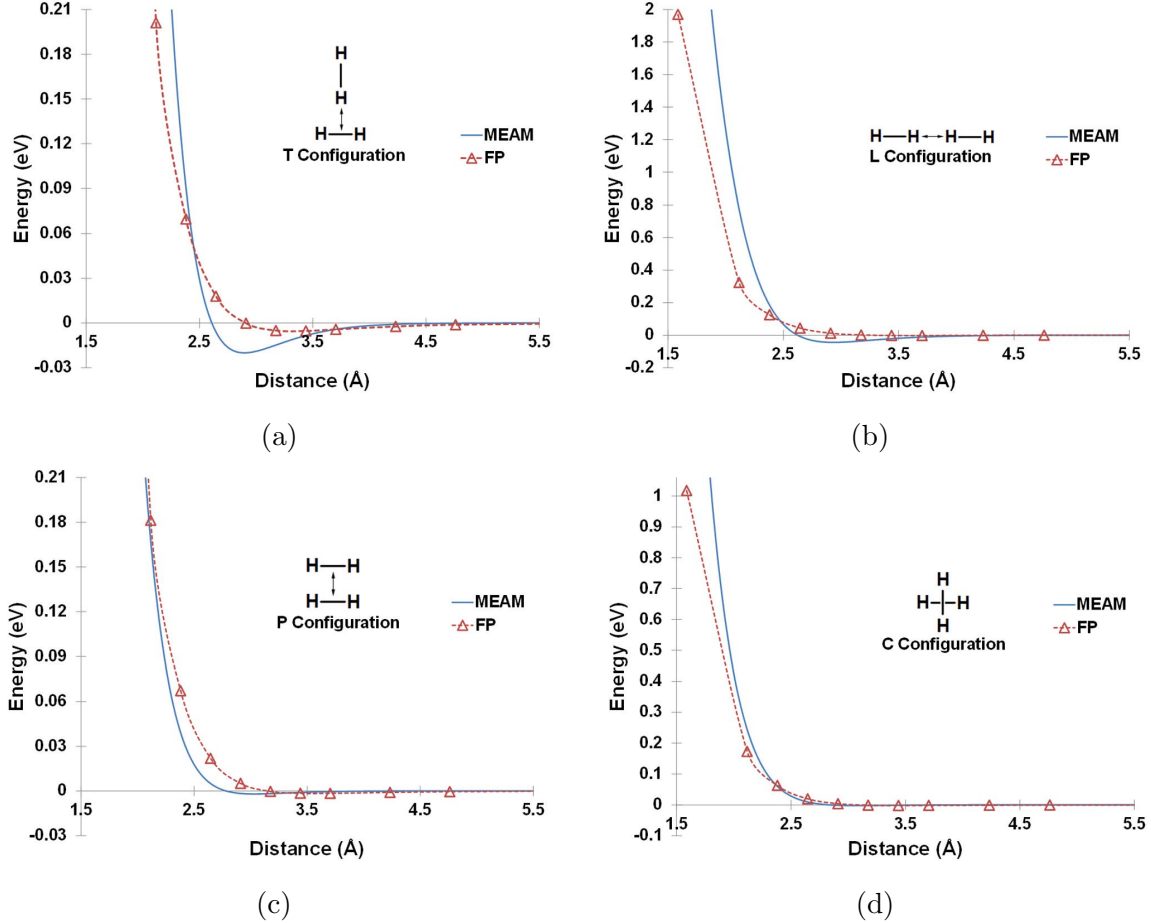


FIG. 6: First-principles (FP)⁴⁵ versus MEAM-calculated interaction energy curves for $(H_2)_2$ (hydrogen dimer). The molecular configurations are a) collinear coplanar (T), b) linear (L), c) parallel or rectangular (P), and d) crossed (C) as reported in the work of Burton et al.⁴⁵. The atoms are constrained during energy calculation at each distance increment.

of future research.

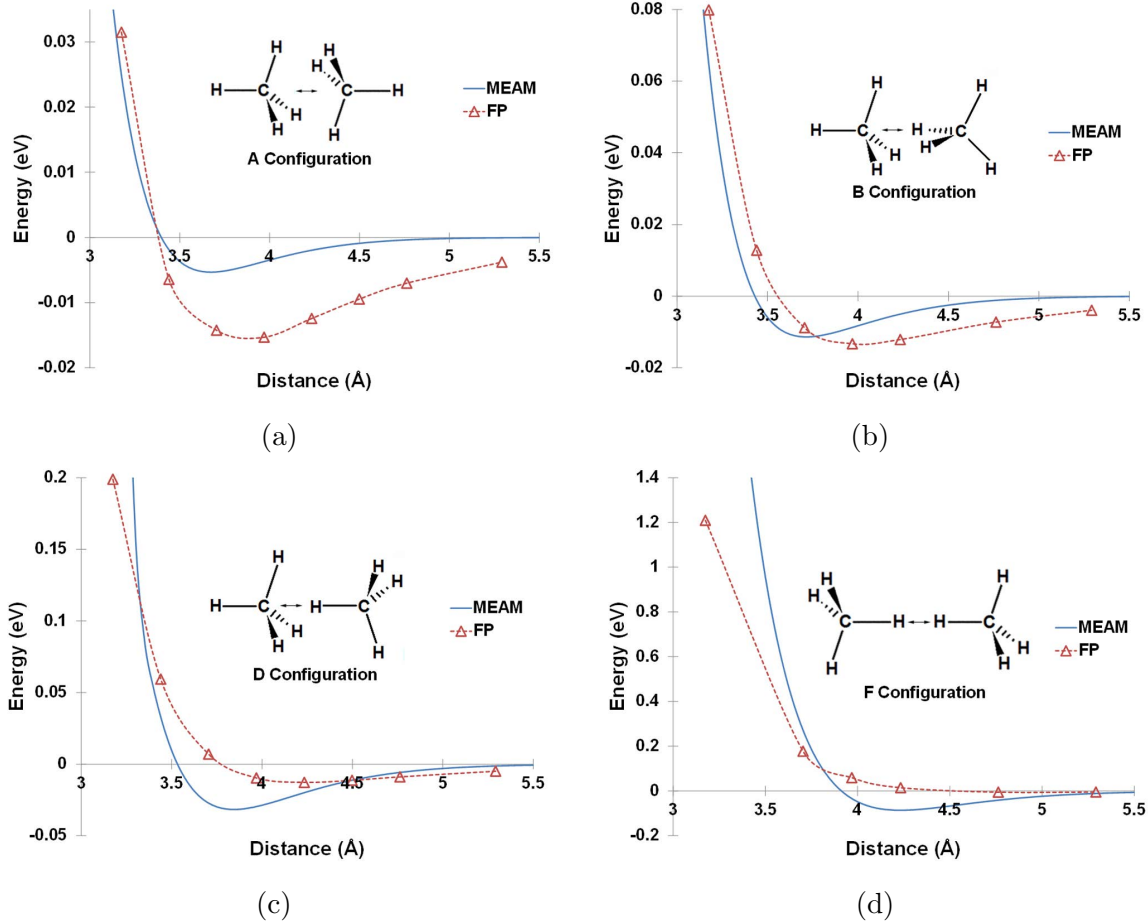


FIG. 7: First-principles (FP)⁴⁶ versus MEAM-calculated interaction energy curves for $(\text{CH}_4)_2$ (methane dimer). The molecular configurations A, B, D, and F are reported in the work of Szczesniak et al.⁴⁶. The atoms are constrained during energy calculation at each distance increment.

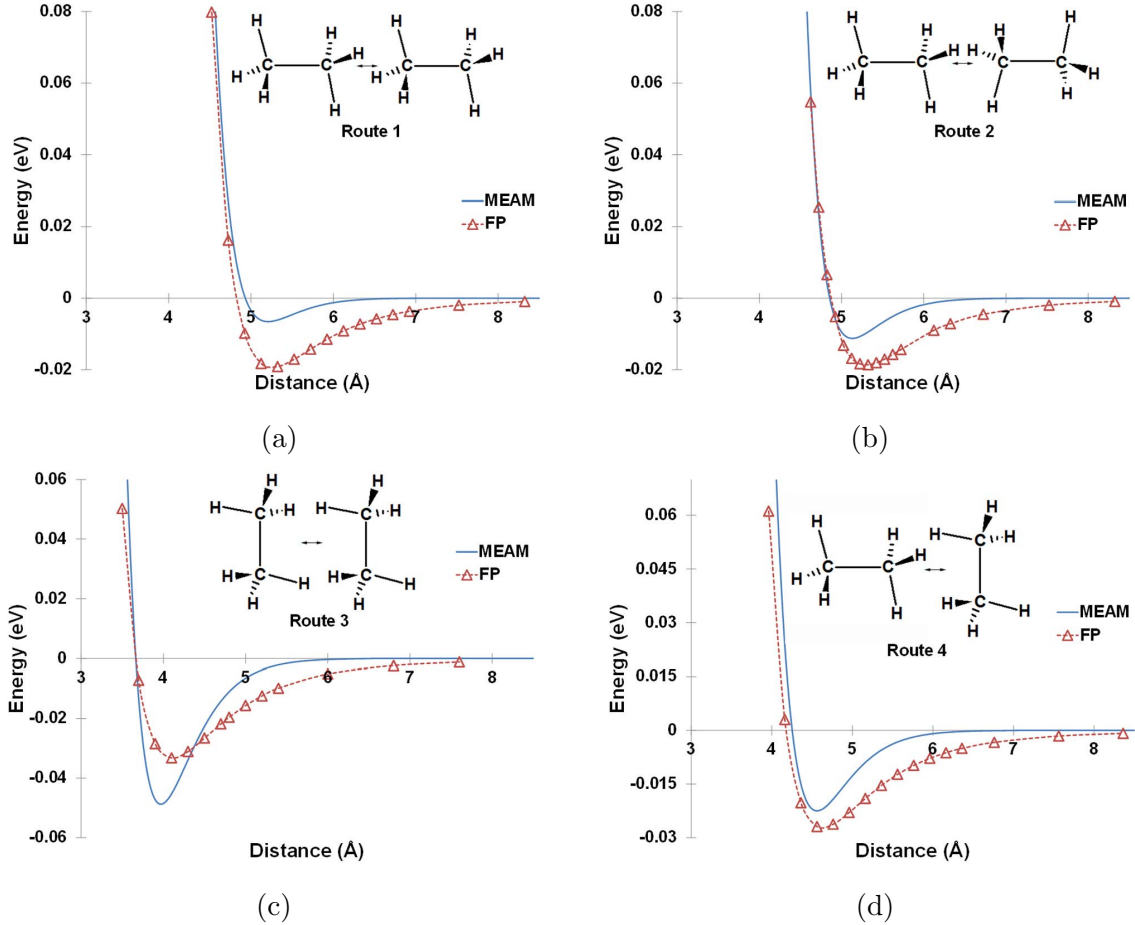


FIG. 8: First-principles (FP)⁴⁷ versus MEAM-calculated interaction energy curves for $(C_2H_6)_2$ (ethane dimer). The molecular configurations (Routes 1-4) are reported in the work of Rowley and Yang⁴⁷. The atoms are constrained during energy calculation at each distance increment.

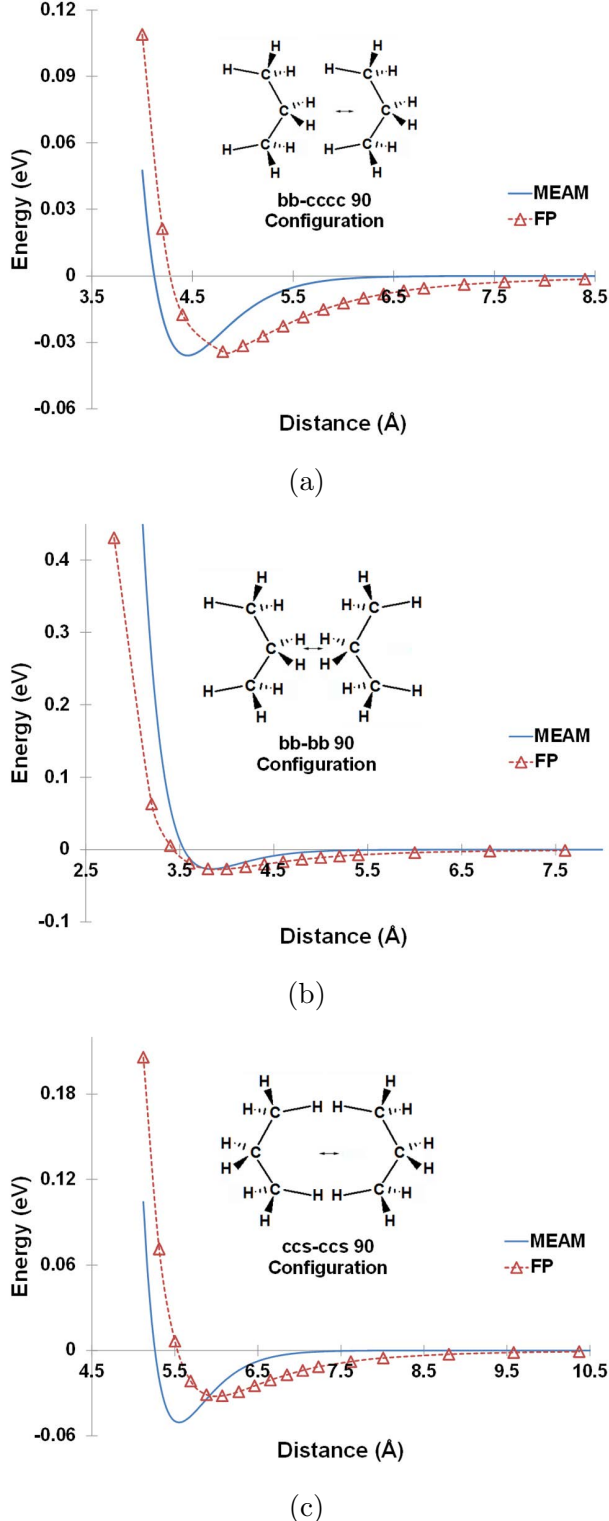
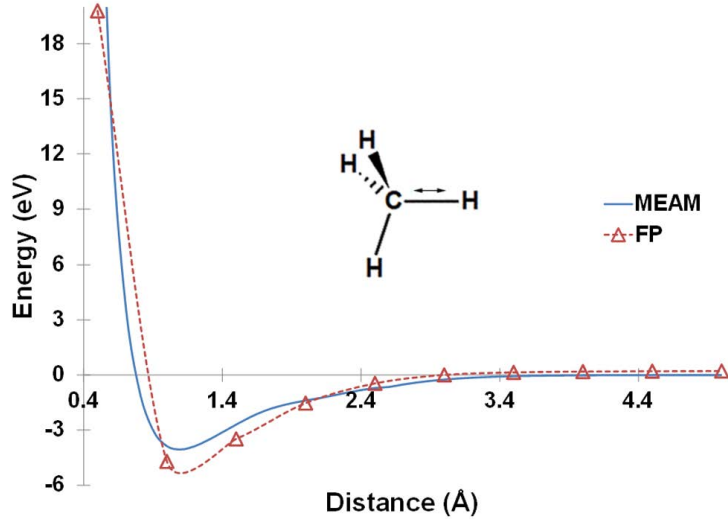
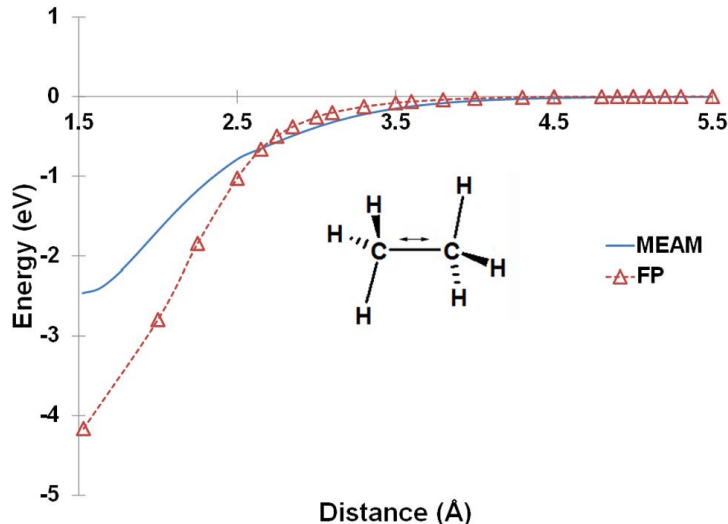


FIG. 9: First-principles (FP)⁴⁸ versus MEAM-calculated interaction energy curves for $(C_3H_8)_2$ (propane dimer). The molecular configurations (bb-cccc 90, bb-bb 90, and ccs-ccs 90) are reported in the work of Jalkanen et al.⁴⁸ The atoms are constrained during energy calculation at each distance increment.



(a)



(b)

FIG. 10: The potential energy curves for the C-H bond dissociation in methane (a) and the C-C bond dissociation in ethane predicted by MEAM versus the FP data. The FP data for a) were generated in this work, while they were taken from the work of Lorant et al.⁶¹ for b). The C and H atoms in CH_4 and both C atoms in C_2H_6 were constrained, while the energy was minimized at each distance increment.

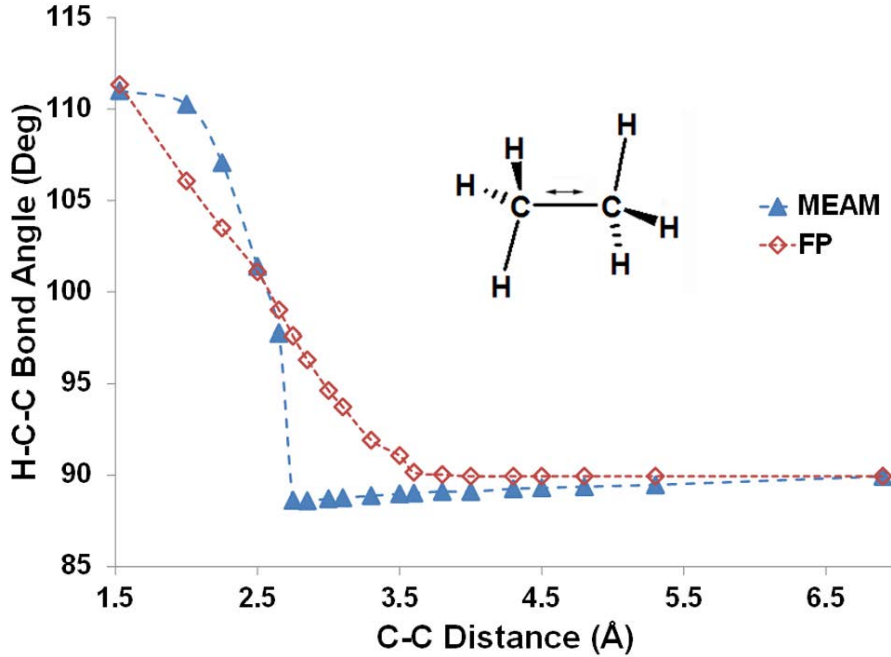


FIG. 11: MEAM-reproduced intermediate H-C-C bond angles during the C-C bond dissociation in ethane compared to the FP data reported in the work of Lorant et al.⁶¹. Both carbon atoms in ethane were constrained, while the energy was minimized at each distance increment.

TABLE VII: Heat of reaction ($\Delta E_{reaction}$) for selected chemical reactions involving C-H and C-C bond breaking reproduced by the MEAM, REBO, and ReaxFF potentials and compared to the experimental data.

Reaction	$\Delta E_{reaction}$ (eV)			
	MEAM	REBO	ReaxFF	Expt. ^a
$\text{CH}_4 \rightarrow \text{CH}_3 + \text{H}^\cdot$	3.745	4.501	4.417	4.484
$\text{C}_2\text{H}_6 \rightarrow \text{C}_2\text{H}_5 + \text{H}^\cdot$	3.715	3.949	4.288	4.313
$\text{C}_3\text{H}_8 \rightarrow \text{CH}_3\text{CH}^\cdot\text{CH}_3 + \text{H}^\cdot$	3.685	3.735	4.634	4.204
$\text{C}_2\text{H}_6 \rightarrow 2\text{CH}_3^\cdot$	2.192	3.827	3.668	3.817
$\text{C}_3\text{H}_8 \rightarrow \text{C}_2\text{H}_5^\cdot + \text{CH}_3^\cdot$	2.158	3.358	3.823	3.774
$\text{C}_4\text{H}_{10} \rightarrow 2\text{C}_2\text{H}_5^\cdot$	2.120	2.888	3.898	3.752
RMS Error ^b	1.23	0.46	0.20	-

^a Calculated from the NIST Computational Chemistry Comparison and Benchmark Database⁴³.

^b Root-Mean-Square Error.

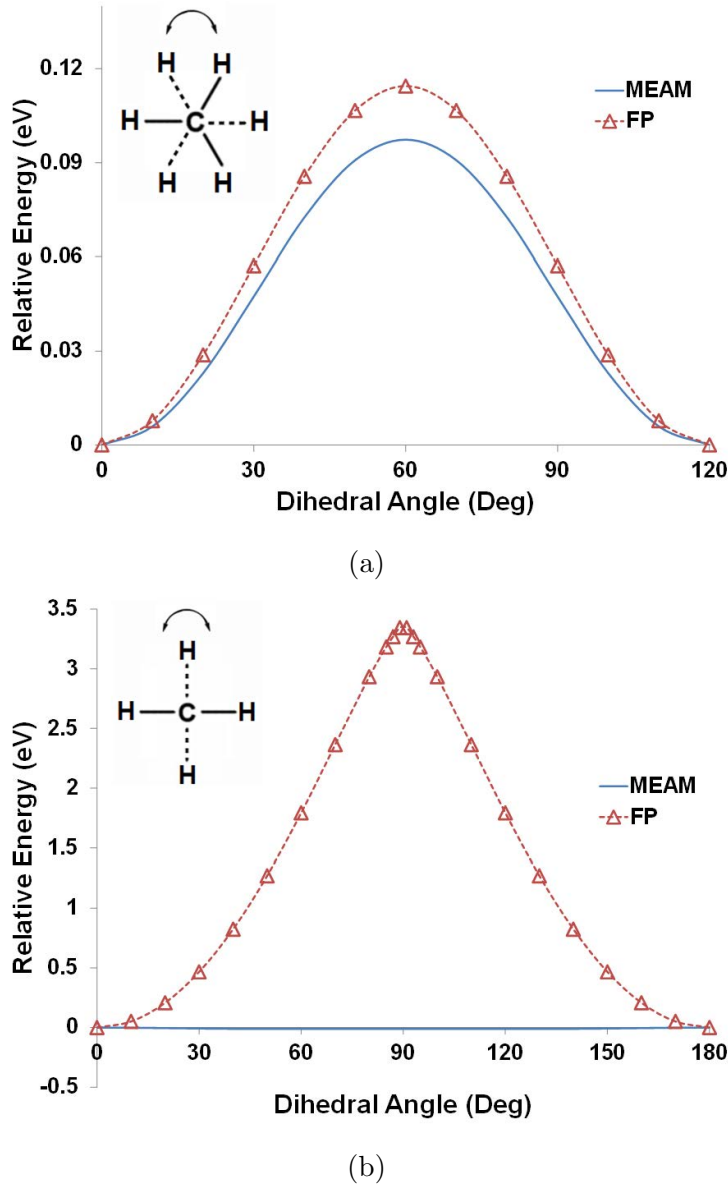


FIG. 12: The rotational barrier for a) ethane and b) ethylene calculated by MEAM versus the FP data calculated using a) CCSD(2)/aug-cc-pVTZ and b) CCSD(T)/aug-cc-pVTZ FP.

E. Molecular dynamics simulations

We further validated our MEAM potential for saturated hydrocarbons with experimental pressure-volume-temperature (*PVT*) data for select alkane systems. The MEAM-calculated pressure for a high-pressure methane system with the density of 0.5534 g/cc was used for fitting purposes. A series of MD simulations were run with *NVT* (constant number of atoms N , constant volume V , and constant temperature T) on a series of 3D periodic methane, ethane, propane, and butane systems with different densities and at different temperatures (Table VIII). The total number of atoms in these systems and the cut-off distance (5 Å) were kept at a minimum due to the large computation times required for running these simulations on the serial DYNAMO⁶⁰ code. To ensure the reliability of the results with a cut-off distance of 5 Å, a representative MD simulation was run on a methane system (density of 0.2021 g/cc) with a larger cut-off distance of 9 Å. The results of both simulations (using cut-off distances of 5 Å versus 9 Å) agree to within 1%. Hence, all the rest of simulations were run using the lower 5 Å cut-off distance. We built the starting periodic structures in Accelrys® Materials Studio® software (V5.5) and relaxed them using the COMPASS³² force field and Polak-Ribiere conjugate gradient method⁵⁶ for 1000 iterations. Then we imported the relaxed periodic structures into DYNAMO and ran the MD simulations on this platform for a total simulation time of 200 ps with a time step of 0.5 fs. The small time step was chosen to ensure energy conservation in these systems containing the light element hydrogen. A typical run took from 6-95 hr on a single processor depending on the size and density of the system. Temperature was controlled by a Nosé-Hoover thermostat^{62,63}. All systems equilibrated after 50 ps. The calculated pressures for each time step were time-averaged over the last 150 ps of the simulation, and an average pressure was calculated. The details of dynamics simulations and the final MEAM-predicted average pressures along with the experimental data are given in Table VIII. In spite of typical uncertainties in experimental data and the fact that a small system was used for the MD simulations, MEAM-reproduced average pressures agree well with the experimental data.

TABLE VIII: Details on the molecular dynamics simulations of a series of periodic methane, ethane, propane, and butane systems under the *NVT* ensemble for a total simulation time of 200 ps. The final MEAM-calculated time-averaged pressure is compared to the experimental data. The data are reported in the ascending order of density for each molecular species.

System	No. of atoms	Cell Size (Å ³)	Density (g/cc)	Temp. (K)	Pressure		
					Expt. (MPa)	MEAM (MPa)	Difference (MPa)
methane-1	500	47.65x47.65x47.65	0.0246	400	5.005 ^a	5.09	0.09
methane-2	500	42.71x42.71x42.71	0.0342	305	5.001 ^a	4.98	-0.02
methane-3	500	28.22x28.22x28.22	0.1185	298	14.994 ^a	12.75	-2.24
methane-4	500	23.62x23.62x23.62	0.2021	450	59.975 ^a	58.65	-1.33
methane-5	500	19.17x19.17x19.17	0.3782	338	179.829 ^a	162.44	-17.39
methane-6	500	18.80x18.80x18.80	0.4008	298	188.059 ^a	173.59	-14.47
methane-7	500	16.88x16.88x16.88	0.5534	373	1000 ^b	1002.41	2.41
ethane-1	800	51.25x51.25x51.25	0.0371	308	2.550 ^c	1.09	-1.46
ethane-2	800	26.36x26.36x26.36	0.2726	308	5.387 ^c	5.57	0.18
ethane-3	800	21.68x21.68x21.68	0.4901	260	31.294 ^c	29.22	-2.07
propane-1	880	28.62x28.62x28.62	0.2497	325	26.891 ^d	4.28	-22.61
propane-2	880	22.40x22.40x22.40	0.5212	280	1.466 ^e	4.49	3.02
<i>n</i> -butane	700	20.23x20.23x20.23	0.5827	300	7.089 ^e	-5.1	-12.19

^a From Cristancho et al.⁶⁴.

^b From Robertson and Babb⁴⁹.

^c From Straty and Tsumura⁶⁵.

^d From Straty and Palavra⁶⁶.

^e From Kayukawa et al.⁶⁷.

V. CONCLUDING REMARKS

We have successfully developed a new semi-empirical many-body potential for saturated hydrocarbons based on the modified embedded-atom method. The potential parameterization was performed with respect to a large database of atomization energies, bond distances, and bond angles of a homologous series of alkanes and their isomers up to *n*-octane, the potential energy curves of H₂, CH, and C₂, (H₂)₂, (CH₄)₂, (C₂H₆)₂, and (C₃H₈)₂ and the pressure-volume-temperature (*PVT*) relationship of a dense methane system. The new potential successfully predicts the *PVT* behavior of representative alkane systems at different densities and temperatures. Furthermore, MEAM predicts the energetics and geometries of the methane and ethane molecules undergoing a bond-breaking reaction reasonably well. The significance of this work is in the extension of the classical MEAM formalism for metals and metal hydride, carbide, and nitride systems to saturated hydrocarbons. This is the first step toward its universality for all atomic and molecular systems. The main benefit of using this potential versus other potentials for various atomic and molecular dynamics simulation studies is its vast parameter database for metals. This makes it possible, for example, to study complex polymer-metal systems using the same formalism for both metals and organic molecules. In addition, MEAM is inherently linear scaling, making possible simulations on very large systems. Since MEAM is a reactive potential, numerous possible simulation studies of reactive organic/metal systems as well as void and crack formation and growth in polymer systems are envisioned.

ACKNOWLEDGMENTS

The authors thank the Department of Energy for partially supporting this work under contract DE-FC26-06NT42755. MAT would like to acknowledge support from the U.S. Army Research Laboratory (ARL).

- ¹ Murray S. Daw and M. I. Baskes. Semiempirical, quantum mechanical calculation of hydrogen embrittlement in metals. *Physical Review Letters*, 50(17):1285–1288, 1983. [1](#), [2](#), [3](#)
- ² M.S. Daw and M.I. Baskes. Embedded-atom method: Derivation and application to impurities, surfaces, and other defects in metals. *Physical Review B*, 29(12):6443, 1984. [1](#), [2](#), [3](#)
- ³ M.S. Daw, S.M. Foiles, and M.I. Baskes. The embedded-atom method: A review of theory and applications. *Materials Science Reports*, 9(7-8):251–310, 1993. [1](#)
- ⁴ MI Baskes. Application of the embedded-atom method to covalent materials: A semiempirical potential for silicon. *Physical Review Letters*, 59(23):2666–2669, 1987. [1](#)
- ⁵ M. I. Baskes. Modified embedded-atom potentials for cubic materials and impurities. *Physical Review B*, 46(5):2727–2742, 1992. [1](#), [2](#), [3](#), [4](#), [6](#), [7](#), [11](#)
- ⁶ M. I. Baskes, J. S. Nelson, and A. F. Wright. Semiempirical modified embedded-atom potentials for silicon and germanium. *Physical Review B*, 40(9):6085–6100, 1989. [1](#)
- ⁷ B.J. Lee and MI Baskes. Second nearest-neighbor modified embedded-atom-method potential. *Physical Review B*, 62(13):8564, 2000. [1](#), [4](#)
- ⁸ B.J. Lee, MI Baskes, H. Kim, and Y.K. Cho. Second nearest-neighbor modified embedded atom method potentials for bcc transition metals. *Physical Review B*, 64(18):184102, 2001. [1](#)

⁹ Byeong-Joo Lee, Jae-Hyeok Shim, and M. I. Baskes. Semiempirical atomic potentials for the fcc metals Cu, Ag, Au, Ni, Pd, Pt, Al, and Pb based on first and second nearest-neighbor modified embedded atom method. *Physical Review B*, 68(14):144112, 2003. [1](#)

¹⁰ MI Baskes, SG Srinivasan, SM Valone, and RG Hoagland. Multistate modified embedded atom method. *Physical Review B*, 75(9):094113, 2007. [1](#)

¹¹ J.M. Zhang, F. Ma, and K.W. Xu. Calculation of the surface energy of fcc metals with modified embedded-atom method. *Applied Surface Science*, 229(1):34–42, 2004. [1](#)

¹² J.M. Zhang, F. Ma, K.W. Xu, and X.T. Xin. Anisotropy analysis of the surface energy of diamond cubic crystals. *Surface and Interface Analysis*, 35(10):805–809, 2003. [1](#)

¹³ MI Baskes and RA Johnson. Modified embedded atom potentials for hcp metals. *Modelling and Simulation in Materials Science and Engineering*, 2:147, 1994. [1](#)

¹⁴ W. Hu, B. Zhang, B. Huang, F. Gao, and D.J. Bacon. Analytic modified embedded atom potentials for hcp metals. *Journal of Physics: Condensed Matter*, 13(6):1193, 2001. [1](#)

¹⁵ J.M. Zhang, F. Ma, and K.W. Xu. Calculation of the surface energy of bcc metals by using the modified embedded-atom method. *Surface and Interface Analysis*, 35(8):662–666, 2003. [1](#)

¹⁶ B. Jelinek, S. Groh, MF Horstemeyer, J. Houze, SG Kim, GJ Wagner, A. Moitra, and MI Baskes. Modified embedded atom method potential for Al, Si, Mg, Cu, and Fe alloys. *Physical Review B*, 85(24):245102, 2012. [1](#), [3](#), [4](#)

¹⁷ H.K. Kim, W.S. Jung, and B.J. Lee. Modified embedded-atom method interatomic potentials for the Fe–Ti–C and Fe–Ti–N ternary systems. *Acta Materialia*, 57(11):3140–3147, 2009. [1](#), [3](#), [4](#)

¹⁸ M.F. Horstemeyer. *Integrated Computational Materials Engineering (ICME) for Metals: Using Multiscale Modeling to Invigorate Engineering Design with Science*. Wiley, 2012. [1](#)

¹⁹ B.J. Lee, W.S. Ko, H.K. Kim, and E.H. Kim. The modified embedded-atom method interatomic potentials and recent progress in atomistic simulations. *Calphad - Computer Coupling of Phase Diagrams and Thermochemistry*, 34(4):510–522, 2010. [1](#), [2](#), [4](#)

²⁰ W. Xiao, MI Baskes, and K. Cho. MEAM study of carbon atom interaction with Ni nanoparticle. *Surface Science*, 603(13):1985–1998, 2009. [1](#), [6](#)

²¹ Jamal Uddin, M. I. Baskes, S. G. Srinivasan, Thomas R. Cundari, and Angela K. Wilson. Modified embedded atom method study of the mechanical properties of carbon nanotube reinforced nickel composites. *Physical Review B*, 81(10):104103, 2010. [1](#)

²² N.L. Allinger, Y.H. Yuh, and J.H. Lii. Molecular mechanics. The MM3 force field for hydrocarbons. 1. *Journal of the American Chemical Society*, 111(23):8551–8566, 1989. [1](#)

²³ J.H. Lii and N.L. Allinger. Molecular mechanics. The MM3 force field for hydrocarbons. 2. Vibrational frequencies and thermodynamics. *Journal of the American Chemical Society*, 111(23):8566–8575, 1989.

²⁴ J.H. Lii and N.L. Allinger. Molecular mechanics. The MM3 force field for hydrocarbons. 3. The van der Waals' potentials and crystal data for aliphatic and aromatic hydrocarbons. *Journal of the American Chemical Society*, 111(23):8576–8582, 1989. [1](#)

²⁵ N.L. Allinger, K. Chen, and J.H. Lii. An improved force field (MM4) for saturated hydrocarbons. *Journal of Computational Chemistry*, 17(5-6):642–668, 1996. [1](#)

²⁶ S.L. Mayo, B.D. Olafson, and W.A. Goddard. DREIDING: A generic force field for molecular simulations. *Journal of Physical Chemistry*, 94(26):8897–8909, 1990. [1](#)

²⁷ D.W. Brenner. Empirical potential for hydrocarbons for use in simulating the chemical vapor deposition of diamond films. *Physical Review B*, 42(15):9458, 1990. [1](#), [10](#), [11](#)

²⁸ D.W. Brenner, O.A. Shenderova, J.A. Harrison, S.J. Stuart, B. Ni, and S.B. Sinnott. A second-generation reactive empirical bond order (REBO) potential energy expression for hydrocarbons. *Journal of Physics: Condensed Matter*, 14:783, 2002. [1](#), [7](#), [9](#), [11](#)

²⁹ A.C.T. Van Duin, S. Dasgupta, F. Lorant, and W.A. Goddard III. ReaxFF: a reactive force field for hydrocarbons. *Journal of Physical Chemistry A*, 105(41):9396–9409, 2001. [1](#), [9](#), [11](#)

³⁰ J. Yu, S.B. Sinnott, and S.R. Phillpot. Charge optimized many-body potential for the Si/SiO₂ system. *Physical Review B*, 75(8):085311, 2007. [1](#)

³¹ T.-R. Shan, B.D. Devine, J.M. Hawkins, A. Asthagiri, S.R. Phillpot, and S.B. Sinnott. Second-generation charge-optimized many-body potential for Si/SiO₂ and amorphous silica. *Physical Review B*, 82(23):235302, 2010. [1](#)

³² H. Sun. COMPASS: An ab initio force-field optimized for condensed-phase applications overview with details on alkane and benzene compounds. *Journal of Physical Chemistry B*, 102(38):7338–7364, 1998. [1](#), [27](#)

³³ W. Somers, A. Bogaerts, A.C.T. van Duin, S. Huygh, K.M. Bal, and E.C. Neyts. Temperature influence on the reactivity of plasma species on a nickel catalyst surface: An atomic scale study. *Catalysis Today*, 211(0):131-136, 2013. [1](#)

³⁴ F. Castro-Marcano and A.C.T. van Duin. Comparison of thermal and catalytic cracking of 1-heptene from ReaxFF reactive molecular dynamics simulations. *Combustion and Flame*, 160(4):766-775, 2013.

³⁵ S. Monti, C. Li, and V. Caravetta. Dynamics Simulation of Monolayer and Multilayer Adsorption of Glycine on Cu(110). *Journal of Physical Chemistry C*, 117(10):5221-5228, 2013.

³⁶ S.-Y. Kim, A.C.T. van Duin, and J.D. Kubicki. Molecular dynamics simulations of the interactions between TiO₂ nanoparticles and water with Na⁺ and Cl⁻, methanol, and formic acid using a reactive force field. *Journal of Materials Research*, 28(03):513-520, 2013. [1](#)

³⁷ T. Liang, B. Devine, S.R. Phillpot, and S.B. Sinnott. Variable Charge Reactive Potential for Hydrocarbons to Simulate Organic-Copper Interactions. *Journal of Physical Chemistry A*, 116(30):7976-7991, 2012. [1](#)

³⁸ T. Liang, Y.K. Shin, Y.-T. Cheng, D.E. Yilmaz, K.G. Vishnu, O. Verners, C. Zou, S.R. Phillpot, S.B. Sinnott, A.C.T. van Duin. Reactive Potentials for Advanced Atomistic Simulations. *Annual Review of Materials Research*, 43:109-129, 2013. [1](#)

³⁹ SM Valone, MI Baskes, and RL Martin. Atomistic model of helium bubbles in gallium-stabilized plutonium alloys. *Physical Review B*, 73(21):214209, 2006. [2](#)

⁴⁰ MI Baskes. Atomistic potentials for the molybdenum-silicon system. *Materials Science and Engineering A*, 261(1):165–168, 1999. [3](#)

⁴¹ J.H. Rose, J.R. Smith, F. Guinea, and J. Ferrante. Universal features of the equation of state of metals. *Physical Review B*, 29(6):2963, 1984. [4](#), [8](#), [9](#)

⁴² D.R. Lide. *CRC handbook of chemistry and physics: a ready-reference book of chemical and physical data*. CRC Press, 2009. [6](#), [10](#), [13](#), [14](#), [15](#)

⁴³ *NIST Computational Chemistry Comparison and Benchmark Database, NIST Standard Reference Database Number 101, Release 15b*. <http://cccbdb.nist.gov/>, August 2011. [6](#), [7](#), [11](#), [25](#)

⁴⁴ Amir Karton, David Gruzman, and Jan M. L. Martin. Benchmark thermochemistry of the C_nH_{2n+2} alkane isomers (n = 2–8) and performance of DFT and composite ab initio methods for dispersion-driven isomeric equilibria. *Journal of Physical Chemistry A*, 113(29):8434–8447, 2009. [6](#), [7](#), [11](#)

⁴⁵ P.G. Burton and U.E. Senff. The (H₂)₂ potential surface and the interaction between hydrogen molecules at low temperatures. *Journal of Chemical Physics*, 76(12):6073–6087, 1982. [6](#), [19](#), [20](#)

⁴⁶ MM Szczesniak, G. Chalansinski, SM Cybulski, and S. Scheiner. Intermolecular potential of the methane dimer and trimer. *Journal of Chemical Physics*, 93:4243, 1990. [6](#), [19](#), [21](#)

⁴⁷ R.L. Rowley, Y. Yang, and T.A. Pakkanen. Determination of an ethane intermolecular potential model for use in molecular simulations from ab initio calculations. *Journal of Chemical Physics*, 114:6058, 2001. [6](#), [19](#), [22](#)

⁴⁸ Jukka-Pekka Jalkanen, Riina Mahlanen, Tapani A Pakkanen, and Richard L Rowley. Ab initio potential energy surfaces of the propane dimer. *Journal of Chemical Physics*, 116:1303, 2002. [6](#), [19](#), [23](#)

⁴⁹ S.L. Robertson and S.E. Babb. PVT properties of methane and propene to 10 kbar and 200°C. *Journal of Chemical Physics*, 51(4):1357–1361, 1969. [6](#), [28](#)

⁵⁰ Steven R Gwaltney and Martin Head-Gordon. A second-order perturbative correction to the coupled-cluster singles and doubles method: CCSD (2). *Journal of Chemical Physics*, 115:2014, 2001. [6](#)

⁵¹ Rick A Kendall, Thom H Dunning Jr, and Robert J Harrison. Electron affinities of the first row atoms revisited. Systematic basis sets and wave functions. *Journal of Chemical Physics*, 96:6796, 1992. [6](#)

⁵² Yihan Shao, Laszlo Fusti Molnar, Yousung Jung, Jorg Kussmann, Christian Ochsenfeld, Shawn T. Brown, Andrew T. B. Gilbert, Lyudmila V. Slipchenko, Sergey V. Levchenko, Daragh P. O'Neill, Robert A. DiStasio Jr, Rohini C. Lochan, Tao Wang, Gregory J. O. Beran, Nicholas A. Besley, John M. Herbert, Ching Yeh Lin, Troy Van Voorhis, Siu Hung Chien, Alex Sodt, Ryan P. Steele, Vitaly A. Rassolov, Paul E. Maslen, Prakashan P. Korambath, Ross D. Adamson, Brian Austin, Jon Baker, Edward F. C. Byrd, Holger Dachsel, Robert J. Doerkens, Andreas Dreuw, Barry D. Dunietz, Anthony D. Dutoi, Thomas R. Furlani, Steven R. Gwaltney, Andreas Heyden, So Hirata, Chao-Ping Hsu, Gary Kedziora, Rustam Z. Khalliulin, Phil Klunzinger, Aaron M. Lee, Michael S. Lee, WanZhen Liang, Itay Lotan, Nikhil Nair, Baron Peters, Emil I. Proynov, Piotr A. Pieniazek, Young Min Rhee, Jim Ritchie, Edina Rosta, C. David Sherrill, Andrew C. Simmonett, Joseph E. Subotnik, H. Lee Woodcock Iii, Weimin Zhang, Alexis T. Bell, Arup K. Chakraborty, Daniel M. Chipman, Frerich J. Keil, Arieh Warshel, Warren J. Hehre, Henry F. Schaefer Iii, Jing Kong, Anna I. Krylov, Peter M. W. Gill, and Martin Head-Gordon. Advances in methods and algorithms in a modern quantum chemistry program package. *Physical Chemistry Chemical Physics*, 8(27):3172–3191, 2006. [6](#)

⁵³ S. R. Gwaltney, Gregory J. O. Beran, and M. Head-Gordon. *Partitioning Techniques in Coupled-Cluster Theory*, volume 1, pages 433–457. Kluwer Academic Publishers, Dordrecht, Netherlands, 2003. [7](#)

⁵⁴ M.D. Hanwell, D.E. Curtis, D.C. Lonie, T. Vandermeersch, E. Zurek, and G.R. Hutchison. Avogadro: An advanced semantic chemical editor, visualization, and analysis platform. *Journal of Cheminformatics*, 4:17, 2012. [7](#)

⁵⁵ Thomas A. Halgren. Merck molecular force field. I. Basis, form, scope, parameterization, and performance of MMFF94. *Journal of Computational Chemistry*, 17(5-6):490–519, 1996. [7](#)

⁵⁶ A. Bhatti. *Practical Optimization Methods: With Mathematica® Applications*. Springer-Verlag, 2000. [7](#), [27](#)

⁵⁷ T. R. Mattsson, J. M. D. Lane, K. R. Cochrane, M. P. Desjarlais, A. P. Thompson, F. Pierce, and G. S. Grest. First-Principles and Classical Molecular Dynamics Simulation of Shocked Polymers. *Physical Review B*, 81(5):054103, 2008. [7](#), [9](#), [11](#)

58 S. Plimpton. Fast parallel algorithms for short-range molecular dynamics. *Journal of Computational Physics*, 117(1):1–19, 1995. [7](#), [11](#), [18](#)

59 K. Chenoweth, A.C.T. van Duin, W.A. Goddard III. ReaxFF reactive force field for molecular dynamics simulations of hydrocarbon oxidation. *Journal of Physical Chemistry A*, 112(5):1040–1053, 2008. [7](#), [9](#)

60 S.M. Foiles, M.S. Daw, and M.I. Baskes. DYNAMO code. *Sandia National Laboratories*, 1994. [9](#), [11](#), [27](#)

61 Franois Lorant, Franoise Behar, William A. Goddard, and Yongchun Tang. Ab initio investigation of ethane dissociation using generalized transition state theory. *Journal of Physical Chemistry A*, 105(33):7896–7904, 2001. [19](#), [24](#), [25](#)

62 Shuichi Nosé. A unified formulation of the constant temperature molecular dynamics methods. *Journal of Chemical Physics*, 81:511, 1984. [27](#)

63 William G Hoover. Canonical dynamics: Equilibrium phase-space distributions. *Physical Review A*, 31(3):1695, 1985. [27](#)

64 D.E. Cristancho, I.D. Mantilla, S. Ejaz, K.R. Hall, M. Atilhan, and G.A. Iglesia-Silva. Accurate $P\rho T$ data for methane from (300 to 450) K up to 180 MPa. *Journal of Chemical & Engineering Data*, 55(2):826–829, 2009. [28](#)

65 GC Straty and R. Tsumura. PVT and vapor pressure measurements on ethane. *J. Res. Natl. Bur. Stand.(US) A*, 80:35–39, 1976. [28](#)

66 GC Straty and AMF Palavra. Automated high temperature PVT apparatus with data for propane. *Journal of Research of the National Bureau of Standards*, 89(5):375–383, 1984. [28](#)

67 Y. Kayukawa, M. Hasumoto, Y. Kano, and K. Watanabe. Liquid-phase thermodynamic properties for propane (1), n-butane (2), and isobutane (3). *Journal of Chemical & Engineering Data*, 50(2):556–564, 2005. [28](#)